Potential additives for magnesia-based concrete with enhanced performance and propensity for CO_2 sequestration

N.T. Dung[a,b], C. Unluer[c,*]

[a] School of Civil and Environmental Engineering, Nanyang Technological University, 50 Nanyang Avenue, Singapore 639798, Singapore

[b] School of Mechanical Aerospace and Civil Engineering, University of Manchester, M1 3NJ Manchester, United Kingdom

[c] School of Engineering, University of Glasgow, G12 8LT, Glasgow, United Kingdom

[*] Corresponding author. E-mail address: Cise.Unluer@glasgow.ac.uk

Abstract

This study focuses on the development of carbonated reactive magnesia cement (RMC) concrete formulations involving hydromagnesite (H), magnesite (M) and hydration agent (HA). Partial replacement of RMC by H and M stimulated the formation of hydrate and carbonate phases. Use of H increased the rate and degree of hydration, resulting in the formation of a bird nest-like structure containing poorly-crystalline brucite. The higher propensity of this poorly-crystalline phase for carbonation increased the utilisation of RMC as a binder and facilitated its conversion into strength-providing HMCs. Synergistic combination of M and HA led to significant strength gain via increased carbonate content and reduced w/b ratio. Presence of M provided micro-aggregates that facilitated the enhanced formation of large carbonate crystals with improved morphologies, resulting in microstructure densification and 113% strength increase. Furthermore, partial replacement of RMC with M enabled reduction of natural resources, CO_2 emissions and energy consumption associated with RMC production.

Keywords: CO_2 sequestration; MgO; additives; performance; microstructure

1. Introduction

Increasing global concerns over high CO_2 emissions and intensive energy and natural resource consumption associated with the production of Portland cement (PC) has led to growing interest in alternative binders with potentially lower environmental impacts. Amongst these alternatives, reactive MgO cement (RMC) presents several advantages such as its ability to absorb CO_2 while gaining strength [1-4], lower calcination temperatures used during its production when compared with PC (750°C vs. ~1400°C) [5], and ability to be fully recycled at the end of its lifetime [6]. The hardening and strength gain mechanisms of RMC-based materials involve the hydration and carbonation processes [7]. Hydration of MgO forms $Mg(OH)_2$, which then reacts with CO_2 to form hydrated magnesium carbonates (HMCs) [8] such as nesquehonite ($MgCO_3 \cdot 3H_2O$), artinite ($MgCO_3 \cdot Mg(OH)_2 \cdot 3H_2O$), hydromagnesite ($4MgCO_3 \cdot Mg(OH)_2 \cdot 4H_2O$) and dypingite ($4MgCO_3 \cdot Mg(OH)_2 \cdot 5H_2O$) [9-13]. The formation of HMCs is associated with the provision of bonding strength and reduction [12] in sample porosity [2], leading to the hardening and strength gain of RMC-based concrete products.

The reactivity of RMC highly depends on the temperature and residence time used during the final calcination process [14, 15]. Accordingly, higher temperatures and/or longer residence times increase the crystallite size of MgO, thereby reducing its reactivity [16, 17]. RMC with a high level of reactivity is produced via the calcination of magnesite at ~700-900°C through the dry-route or the calcination of brucite at ~500-700°C through the wet-route [18-21].

In addition to the reactivity of RMC, the performance of RMC-based samples highly depends on the hydration and carbonation processes. The slow dissolution of MgO and the precipitation of hydration products on its surface limit the further contact of unreacted particles with water, hindering the continuation of the hydration process and associated strength gain [22-25]. The use of hydration agents (e.g. magnesium acetate ($Mg(CH_3COO)_2$) or magnesium chloride ($MgCl_2$)) and high-temperature pre-curing are two methods that can increase the hydration degree of RMC from ~50% to ~80%. Subjecting RMC samples to accelerated carbonation curing (5-20% CO_2) can also improve their toughness and stiffness, thereby increasing their 28-day compressive strength to > 20 MPa [11, 26-30]. The simultaneous use of a hydration agent and accelerated carbonation led to RMC concrete samples with strengths as high as ~60 MPa [24, 31]. Even higher strengths were obtained under the simultaneous inclusion of nucleation seeding and hydration agent/sodium bicarbonate ($NaHCO_3$), which enhanced the

hydration and carbonation reactions and led to compressive strengths of ~70 MPa in RMC formulations [28, 32, 33]. Previous studies [10, 31] showed that RMC-based samples cured under accelerated carbonation gained higher compressive strengths than corresponding PC-based samples.

Despite these improvements in the performance of carbonated RMC concrete samples, a large amount of unreacted MgO and $Mg(OH)_2$ was present in the sample composition even after 28 days of curing [10, 28, 33-36]. The low conversion of MgO or $Mg(OH)_2$ to HMCs was attributed to the formation of an impervious layer of HMCs during the initial carbonation reaction, which limited the further diffusion of CO_2 from the outer surface towards the sample core [37, 38]. For this reason, only a fraction of the CO_2 emitted during the production of RMC could be re-absorbed in these concrete samples, which were initially aimed to be sustainable alternatives to PC.

Another approach focused on blending RMC with hydromagnesite (H) to form a hydraulic RMC-H cement with lower CO_2 emissions [3, 39, 40]. The inclusion of 10-30% H within these samples significantly accelerated the hydration of RMC at early stages, resulting in earlier setting and a noticeable strength gain (i.e. ~25 MPa at 28 days) [3, 41, 42]. This significant increase in strength was attributed to the higher content of hydrate phases with improved morphologies within RMC-H samples when compared to RMC samples [41, 43]. However, high amounts of unreacted MgO and $Mg(OH)_2$ were still observed in RMC-H samples after 28 days of curing, revealing the ineffective use of RMC as a binder. Furthermore, the high amounts of unreacted MgO and $Mg(OH)_2$ could cause concerns about volume stability in the long-term as these phases could hydrate and carbonate at later ages, potentially causing excessive expansion. While previous studies reported that the low-crystallinity $Mg(OH)_2$ froming in RMC-H samples could be prone to carbonation [44], the extent of this under a CO_2 intensive environment has not been investigated. As these disadvantages could inhibit the application of RMC in the construction industry, it is critical to identify solutions for improving the utility and hence the carbonation potential of RMC, which will enable higher degrees of CO_2 sequestration and lower carbon footprints.

When compared to the use of H in RMC-H blends, magnesite (M, $MgCO_3$) is a more cost-effective and viable additive. This is not only because M has much more abundant natural resources than H, but it can also be produced via the carbonation of magnesium

silicate minerals (e.g. serpentine ($Mg_3Si_2O_5(OH)_4$) and olivine (Mg_2SiO_4)), which have large amounts of global reserves around the world [45-47]. The process of transforming magnesium silicate minerals into M requires high temperatures and pressures, necessitating the development of an energy-efficient industrial process [43, 48]. When scaled up, this route will present a promising route for the production of M from magnesium silicate minerals, which will reduce CO_2 emissions associated with cement production. Furthermore, the simultaneous use of magnesium acetate and M was reported to improve the compressive strength of RMC samples by 240% [44]. While these advantages make M an attractive material to be used in RMC formulations, its influence on the carbonation mechanisms, and associated performance and microstructural development has not been studied until now.

In line with this gap in the literature, this study aims to develop sustainable RMC-H (i.e. RMC with hydromagnesite) and RMC-M (i.e. RMC with magnesite) concrete formulations with a high utilization rate of RMC, which was enabled by the partial replacement of RMC with H and M, respectively. Within these formulations, a majority of the unreacted MgO and $Mg(OH)_2$ were transformed into HMCs, thereby enhancing performance and facilitating the effective use of RMC as a binder. The increased transformation of unreacted MgO and $Mg(OH)_2$ into HMCs was made possible via (i) the use of magnesium acetate tetrahydrate ($(CH_3COO)_2Mg{\cdot}4H_2O$) as a hydration agent (HA) to improve the conversion of MgO into $Mg(OH)_{2(aq,s)}$ available for carbonation; and (ii) the increase in carbobation in the presence of carbonates that improved the conversion of MgO/$Mg(OH)_{2(aq,s)}$ into HMCs. To evaluate the properties of the final mixes, a comprehensive investigation on the effects of H and M on the hydration and carbonation of RMC was performed. The hydration kinetics of RMC in the presence of HA, H and M were assessed via isothermal calorimetry. The performance of RMC-H and RMC-M concrete samples with and without HA under ambient and accelerated carbonation conditions was evaluated via the measurement of their compressive strengths at different durations. These results were further supported by a detailed microstructural characterization involving the use of x-ray diffraction (XRD), thermogravimetry-infrared spectroscopy (TG-IR), differential thermogravimetry (DTG), scanning electron microscopy (SEM), Energy Dispersive X-Ray (EDX) and backscattered electron (BSE) analyses, which enabled the assessment of hydration and carbonation products within the prepared formulations.

2. Materials and Methodology

2.1 Materials

Commercial RMC (obtained from Richard Baker Harrison-UK), with the chemical composition and physical properties given in Table 1, was used in this study. Commercial H and M (both obtained from Fisher Scientific-UK), used as partial replacements of RMC in the prepared blends, had specific surface areas (SSA) of 43.5 and 2.3 m^2/g, respectively. The particle size distributions and the XRD patterns of RMC, H and M are shown in Fig. 1 and 2, respectively. The low calcination temperatures used during the production of RMC often lead to the presence of uncalcined magnesite in the final product, explaining the magnesite reflections at 32.8° and 42.9° 2θ in Fig. 2, which overlapped with RMC. The morphologies of these materials, shown in Fig. 3, revealed the angular and irregular grains of RMC. Alternatively, H indicated spherical agglomerations of disk-like crystals and M was composed of cubic particles. HA (obtained from VWR-Singapore) was included in the prepared mixes to improve the conversion of RMC into hydrate and carbonate phases [31, 33]. Saturated surface dry gravel with a particle size of ~5-10 mm was used as aggregates in concrete samples. Fine aggregates were not included in the mix design to enable the extraction of pastes from the concrete samples without any contamination and to assure the accurate quantification of hydration and carbonation phases.

2.2 Sample preparation

Six concrete mixtures were prepared to investigate the influence of H and M on the hydration and carbonation of RMC with and without HA. Based on preliminary studies and the findings of previous research [41, 43], H and M replaced RMC by 20% and 40% by mass to accelerate the hydration of RMC, respectively. The details of all mix compositions are shown in Table 2. The first three samples did not include any HA. The control sample (CS), whose binder was only composed of RMC, was prepared with a water/binder (w/b) mass ratio of 0.6. With the goal of achieving a similar workability level as the CS, the replacement of 20% RMC with H led to an increase in the w/b ratio to 1.2 in sample RMC-H due to the high surface area of H. This higher water content of sample RMC-H resulted in a lower aggregate content when compared with the CS. In contrast, the replacement of 40% RMC with M resulted in a reduction

in the w/b ratio to 0.55 in sample RMC-M, due to the low surface area of M. The last three samples were composed of the same binder compositions as the first three, with the only difference of including HA at a concentration of 0.05 M in their mix design, to accelerate the hydration and carbonation of RMC.

To prepare the concrete samples, the binder was first mixed with water or HA solution (i.e. prepared by dissolving HA in the mixing water), forming a homogeneous paste, followed by the introduction of aggregates. The concrete samples were then cast into 5 cm cube moulds, consolidated and surface leveled. All the prepared samples were cured under ambient conditions (i.e. ~30°C and ~75-80% relative humidity (RH)) for 2 days. After de-moulding, one set of samples was continuously cured under ambient conditions, while another set was cured under accelerated carbonation conditions (i.e. 10% CO_2, ~30°C and ~75-80% RH), for a total of 28 days.

2.3 Methodology

The influence of the additives (i.e. HA, H and M) on the hydration of RMC was demonstrated by the heat flow released by each mix at 30°C, which was measured by an I-Cal 8000 high precision calorimeter [49]. The water or HA solution and binders were pre-heated to 30°C for 24 hours prior to mixing to obtain the same conditions as those used during the curing process. After mixing, the prepared pastes were immediately placed into individual calorimeter chambers to record the heat flow of hydration for 24 hours.

The compressive strengths of the concrete samples were measured at a loading rate of 55 kN/min on a Toni Technik Baustoffprüfsysteme machine. Three samples were tested for each data point and their average and standard deviation were reported.

The paste segments extracted from the exterior of samples subjected to compressive strength testing were stored in isopropanol for 24 hours and dried under vacuum for microstructural analysis. The details of this procedure used to prepare samples for microstructural analysis were provided in previous studies [50, 51]. XRD and TG-IR analyses were performed on ground powder samples with particle sizes less than 75 μm. XRD was performed on a Philips

PW 1800 spectrometer using Cu K_α radiation (40 kV, 30 mA) at a scanning rate of 0.04° 2θ/step, operated from 5° to 70° 2θ.

TG was performed on a Perkin Elmer TGA 4000, operated from 30°C to 920°C at a heating rate of 10 °C/min and a flow rate of 20 ml/min, under N_2. The hydrate phases within each sample were quantified by deconvoluting the DTG curves to obtain the area corresponding to the decomposition of each phase. The outlet of the Perkin Elmer TGA 4000 equipment was coupled with a Perkin Elmer Fourier Transform Infrared (FT-IR) spectrometer via a Perkin Elmer TG-IR TL 8000 interface. This interface transferred the evolved gases from the TG equipment to the FT-IR spectrometer to provide information regarding the gases released during thermal decomposition. The transfer line and IR cell were maintained at 150°C to prevent condensation on the windows. The IR spectra were recorded in the spectral range of 4000–450 cm^{-1}, with a 4 cm^{-1} resolution and 16 scans. The IR absorbances of H_2O and CO_2 released during thermal decomposition were identified in the rages of ~3400-4000 cm^{-1} and ~2250-2450 cm^{-1}, respectively. To quantify the mass loss at each step of decomposition, DTG curves were deconvoluted based on the IR absorbance peaks of H_2O and CO_2 by using the Gaussian area deconvolution method and Origin 2017 software.

SEM images were obtained by a Zeiss Evo 50 microscope to investigate the morphologies of the hydration and carbonation products that formed within the prepared samples under ambient and accelerated carbonation conditions. The elemental distributions were obtained by EDX with an accelerating voltage of 15 kV and a working distance of 17 mm. BSE imaging was also performed to investigate the sample microstructure and phase formations within selected samples. In preparation for BSE analysis, the vacuum dried samples were mounted in epoxy resin impregnation under vacuum for 24 hours and polished to obtain smooth surfaces. Sandpaper was used prior to final polishing by diamond slurry with sizes of 9, 3, 1 and 0.3 μm. The polished samples were cleaned with isopropanol in an ultrasonic bath for 10 minutes. The samples were then dried for 24 hours under vacuum and exposed to compressed air jet to remove any remaining dust from their surfaces before coating with gold prior to analysis.

3. Results

3.1 Isothermal calorimetry

Fig. 4 shows the heat flow released during the first 24 hours of hydration within all samples. The results were normalized with respect to the RMC content. The heat release associated with the dissolution of MgO (i.e. the main phase present in RMC) was observed in all samples after mixing. The higher exothermal peaks of samples RMC-H and RMC-M than that of the CS revealed the role of H and M in accelerating the hydration of RMC within these samples (Fig. 4(a)). The higher surface area of H could have stimulated the nucleation and growth of hydrate phases, thereby explaining its highest exothermal peak when compared with the CS and RMC-M samples.

As can be seen in Fig. 4(b), the introduction of HA into RMC formulations led to a very obvious increase in the heat flow associated with the hydration process. Within this second set of mixes involving the use of HA, the replacement of RMC with M in sample HA.RMC-M did not influence the hydration reaction, whereas the use of H in sample HA.RMC-H had an obvious effect on the heat release. Accordingly, the simultaneous inclusion of HA and H revealed the highest exothermal peak within sample HA.RMC-H, followed by a slightly lower heat release than samples HA.RMC-M and HA.CS after ~6 hours of hydration. The increase in the initial stages of hydration could be attributed to the enhancement of the dissolution of MgO, followed by the nucleation and growth of hydrate phases in the presence of H, whose large surface area could have enanced these processes by acting as a nucleation seed.

Fig. 5 presents the cumulative heat of all samples after 24 hours of hydration. The accelerated hydration of RMC when included with H and M resulted in higher cumulative heat in samples RMC-H and RMC-M when compared with the CS (Fig. 5(a)). Among samples involving HA, the lower rate of hydration at later stages led to the lowest culmulative heat after 16 hours of hydration in sample HA.RMC-H (Fig. 5(b)). Alternatively, the inclusion of M or H did not seem to affect the rate and cumulative heat of samples incorporating HA.

3.2 Compressive strength

The strength development of concrete samples cured under ambient and accelerated carbonation conditions for up to 28 days is shown in Fig. 6(a) and (b), respectively. Amongst

samples subjected to ambient conditions (Fig. 6(a)), the CS produced a compressive strength of ~5 MPa after 28 days of hydration. The inclusion of 40% M increased the 28-day compressive strength of sample RMC-M to 6 MPa. Despite its obvious effect in accelerating the hydration of RMC (Fig. 4(a)), the use of H in sample RMC-H produced the lowest strengths (< 4 MPa) amongst all samples. This inconsistency in the strength results could be attributed to the higher w/b ratio of sample RMC-H, which may have increased its porosity, thereby leading to lower strengths. In line with the isothermal calorimetry results, the use of HA resulted in noticeable strength gains in samples HA.CS, HA.RMC-H and HA.RMC-M. Amongst these, sample HA.RMC-H reached 6 MPa at 2 days and increased to 8 MPa at 28 days, while the compressive strength of sample HA.CS remained at ~8 MPa throughout the entire curing period. Outperforming all the others, sample HA.RMC-M demonstrated a noticeable strength development starting with early ages and reached ~13 MPa at 14 days.

Consistent with the findings of previous studies [25, 31, 52-54], the reaction with CO_2 significantly enhanced the strength development of all samples, which was associated with the formation of HMCs (Fig. 6(b)). Most samples, except for HA.RMC-M, demonstrated rapid strength gains during the first seven days, followed by a plateau. Accordingly, the CS reached a strength of 23 MPa after 7 days, after which this value remained stable. Sample RMC-M followed a very similar trend to the CS during the entire curing period. Similar to the trend observed in ambient curing conditions, sample RMC-H revealed lower strength results of 16 MPa at 28 days, which did not increase via the incorporation of HA in sample HA.RMC-H. This could be an indication of the limitations in the strength development of this mix in line its high w/b ratio. On the other hand, the use of HA led to higher compressive strengths in sample HA.CS than the CS (27 vs. 23 MPa at 28 days). Differing from other samples, HA.RMC-M demonstrated a continuous increase in strength throughout the entire curing duration, showing that the simultatneous inclusion of HA and M could enhance the hydration and carbonation reactions and result in a significant strength gain (49 MPa at 28 days). Therefore, when coupled with the use of HA, the replacement of 40% RMC with M not only produced a more sustainable binder by enabling the replacement of RMC with a naturally occuring carbonate (i.e. magnesite), but also resulted in notably better performance than purely RMC-based samples.

3.3 Microstructure

Fig. 7 reveals the microstructures of all samples after 2 days of curing under ambient conditions. The CS (Fig. 7(a)) presented sparsely hydrated MgO grains, where the precipitation of brucite on the MgO surfaces could have inhibited the further hydration of MgO, resulting in a porous microstructure. When compared with the CS, the use of H in sample RMC-H (Fig. 7(b)) led to the formation of disk-like crystals with a diameter of ~0.5 μm, which were firmly linked into larger crystals. Alternatively, the combination of RMC and M in sample RMC-M (Fig. 7(c)) resulted in the formation of smaller crystals away from MgO grains. These crystal particles could have acted as nucleation sites for the precipitation of brucite on their surfaces in the pore space, resulting in a denser microstructure than the CS. Sample HA.CS (Fig. 7(d)) revealed the densest microstructure amongst all samples, which could have been attributed to the increased formation of hydrate phases in the presence of HA. The simultaneous inclusion of HA and H in sample HA.RMC-H (Fig. 7(e)) resulted in crystals with larger sizes; whereas the use of HA and M in sample HA.RMC-M (Fig. 7(f)) led to a widespread formation of hydrate agglomerates. These changes in the microstructures of samples HA.RMC-H and HA.RMC-M could explain their improved performance in comparison to corresponding samples without any HA (RMC-H and RMC-M), respectively. Investigation of the microstructures of the same samples after 28 days of curing under the same conditions revealed similar patterns (Fig. 8). Accordingly, as hydration proceeded, an increased formation of hydrates with larger crystal sizes was generally observed, leading to denser microstructures at 28 days.

Subjecting the samples to accelerated carbonation significantly improved their microstructures, as shown in Fig. 9. All samples revealed the formation of various HMCs, which can explain the noticeable improvement in the strength gain of carbonated samples. The rosette-like hydromagnesite/dypingite agglomerates composed of plate-like crystals with a diameter of ~3-4 μm was observed in the CS (Fig. 9(a)) [55, 56]. The inclusion of 20% H led to the widespread formation of hydromagnesite/dypingite with smaller diameters of ~2-3 μm in sample RMC-H (Fig. 9(b)). The use of 40% M resulted in the formation of hydromagnesite/dypingite agglomerates that were similar to those observed in the CS (~4-5 μm in diameter) in sample RMC-M (Fig. 9(c)). Differing from other samples, the use of HA stimulated the formation of large nesquehonite crystals (~0.5 μm in diameter and up to ~10 μm in length) surrounding other hydrate and carbonate phases in sample HA.CS (Fig. 9(d)). The combination of HA and H in sample HA.RMC-H revealed a very similar microstructure (Fig. 9(e)) as that of sample RMC-H (Fig. 9(b)), which could explain their similar performances under accelerated carbonation

conditions. Alternatively, the simultaneous inclusion of HA and M in sample HA.RMC-M led to the establishment of a very dense structure composed of thick wall-like structures of nesquehonite crystals that were bridged together by hydromagnesite/dypingite crystals (Fig. 9(f)). This significant change when compared with the microstructure of sample RMC-M (Fig. 9(c)) was in line with the differences in the strength results, in which sample HA.RMC-M remarkably outperformed all other samples.

In line with these microstructural observations, some carbonated samples were chosen for further investigation via BSE, as shown in Figs. 10-12. Amongst these samples, the microstructure of the CS was dominated by unhydrated RMC grains with a diameter of up to ~35 μm (Fig. 10(a)). The use of HA and/or M accelerated the hydration of RMC, resulting in unhydrated RMC particles with smaller sizes (< 20 μm) in samples HA.CS (Fig. 10(b)), RMC-M (Fig. 10(c)) and HA.RMC-M (Fig. 10(d)). An interesting formation of a poorly crystalline/amorphous structure was revealed in carbonated samples RMC-H (Fig. 11) and HA.RMC-H (Fig. 12). Within these samples, a bird nest-like arrangement, in which the round H seeds were surrounded by the agglomeration of disk-like crystals, was observed. This unique formation, which was not reported in the prior carbonated RMC-related literature until now, was composed of magnesium and carbon, as shown in the elemental analysis results (Figs. 13 and 14).

3.4 XRD

The XRD patterns of of all samples subjected to ambient conditions and accelerated carbonation are presented in Figs. 15 and 16, respectively. In addition to unhydrated MgO (42.9° and 58.7° 2θ), brucite (18.6°, 38.1° and 50.9° 2θ) and pokrovskite ($Mg_2CO_3(OH)_2$; main reflection at 17.2° and 32.8° 2θ [57, 58]) were observed in all samples after 2 days of hydration under ambient conditions (Fig. 13). A comparison of the hydrated phases within samples based on the intensity of the internal standard, CaF_2 (main reflection at 28.2° 2θ), indicated the increase in the hydration of MgO and associated formation of phases such as brucite, in the presence of HA. The accelerated formation of brucite stimulated its reaction with CO_2, resulting in the higher formation of pokrovskite in sample HA.CS than CS under ambient conditions. The inclusion of H led to broad reflections of brucite within samples RMC-H and HA.RMC-H, indicating the presence of poorly crystalline/amorphous $Mg(OH)_2$ within these

samples, which was in line with the BSE observations shown in Figs. 11 and 12. Alternatively, the inclusion of M did not lead to a significant change in the composition of hydrated products when compared with the CS. The occurrence of calcite ($CaCO_3$, main reflection at 29.7° 2θ) within these samples was attributed to its presence as an impurity in M.

Use of accelerated carbonation revealed an increase in the pokrovskite content of the CS (Fig. 16). The reduction in the amounts of brucite and pokrovskite in sample HA.CS could be attributed to their transformation into other HMCs under accelerated carbonation. The broad reflections of brucite observed in samples RMC-H and HA.RMC-H under ambient conditions disappeared after accelerated carbonation. This change could be associated with the higher propensity of these poorly crystalline/amorphous $Mg(OH)_2$ phases to carbonate than brucite crystals. The disappearance of these broad reflections around brucite was accompanied with the obvious formation of dypingite at 8.3° 2θ and hydromagnesite at 15.3° 2θ, along with a reduction in MgO content in samples RMC-H and HA.RMC-H. Therefore, the inclusion of H in RMC formulations not only enabled the formation of amorphous $Mg(OH)_2$ that was prone to carbonation, but also stimulated the utilisation of MgO in hydration/carbonation reactions. Similarly, samples RMC-M and HA.RMC-M demonstrated reductions in brucite and pokrovskite contents under accelerated carbonation. However, the presence of reflections corresponding to HMC phases was not clearly observed in the XRD patterns of these samples due to their low intensities, in spite of their very obvious presence revealed by the SEM images (Fig. 9).

3.5 TG-IR & DTG

TG-IR results of prepared samples cured under ambient and accelerated carbonation conditions are shown in Figs. 17 and 18, respectively. Under ambient conditions (Fig. 17), the majority of the mass loss observed in the CS was attributed to the dehydroxylation of brucite and HMCs (e.g. pokrovskite) at ~420°C [59], in addition to the decarbonation of carbonate phases at ~400°C, 580°C and 680°C (Fig. 17(a)). The inclusion of H and M in samples RMC-H (Fig. 17(b)) and RMC-M (Fig. 17(c)) led to an increase in the amount of mass loss corresponding to decarbonation at ~460°C and 650°C, accompanied by a smaller mass loss due to dehydroxylation at 400°C. The use of HA in sample HA.CS (Fig. 17(d)) resulted in higher total mass loss than CS, albeit presenting similar patterns of dehydration and decarbonation. When

compared with sample RMC-H, the simultaneous inclusion of HA and H in sample HA.RMC-H (Fig. 17(e)) increased the total mass loss without altering the dehydroxylation and decarbonation patterns. Alternatively, the combined use of HA and M in sample HA.RMC-M (Fig. 17(f)) not only increased the total mass loss associted with the decomposition of hydrate and carbonate phases, but also shifted the main decarbonation peak to ~600°C in comparison to sample RMC-M.

Samples subjected to accelerated carbonation led to significantly increased total mass loss values (Fig. 18). IR results indicated that this increase in mass loss was attributed to the decarbonation process within each sample. Accordingly, the inclusion of H in samples RMC-H and HA.RMC-H led to a noticeable increase in mass loss corresponding to decarbonation, indicating the significant improvement in CO_2 sequestration within these samples. The decarbonation of samples CS and HA.CS mostly peaked at ~400°C ((Fig. 18(a) and (d)), while that of samples RMC-H and HA.RMC-H peaked at ~480°C ((Fig. 18(b) and (e)). On the other hand, two major peaks at ~400°C and ~600°C corresponding to decarbonation were revealed by samples RMC-M and HA.RMC-M ((Fig. 18(c) and (f)). The high intensities of these peaks highlighted the increased formation of carbonate phases within these samples, along with the decomposition of M included in the original mix design.

The mass loss values corresponding to different decomposition steps revealed by TGA and calculated by the deconvolution of the DTG curves (Figs. 19 and 20) based on the IR results as detailed in Section 2.3, are summarized in Tables 3 and 4 for samples cured under ambient and carbonated conditions, respectively. The majority of the recorded mass loss was attributed to the (i) dehydroxylation (of brucite and carbonate phases), (ii) decarbonation (of carbonates) and (iii) dehydration (of water bonded to HMCs) steps. Amongst all samples subjected to ambient conditions (Table 3), CS revealed the lowest mass loss values. Accordingly, the small amount (0.7%) of mass loss corresponding to dehydration revealed the low carbonation degree of the CS, whereas the presence of uncalcined magnesite in RMC and the partial formation of HMCs were responsible for 13.4% mass loss associated with decarbonation observed in this sample. The higher mass loss observed during the dehydration and decarbonation steps of sample RMC-H was attributed to the decomposition of H. The inclusion of M in sammple RMC-M revealed a higher mass loss during decarbonation, which was mainly associated with the decompostion of M. The use of HA significantly accelerated the hydration and carbonation of samples even under ambient conditions. This enhancement in the reaction mechanisms was

indicated by the notable increase in the mass loss corresponding to dehydration and decarbonation steps within samples HA.CS, HA.RMC-H and HA.RMC-M when compared with samples without any HA (i.e. CS, RMC-H and RMC-M), respectively. These findings were in line with the advancements observed in the strength results, highlighting the role of HA in enhancing the mechanical performance of RMC, RMC-H and RMC-M formulations.

When the samples subjected to accelerated carbonation were observed (Table 4), a significant increase in the mass loss of all samples due to dehydration and decarbonation was revealed. Amongst these, the CS and HA.CS experienced the lowest increase, whereas those involving H and M led to much higher mass loss values, mainly highlighting the increased formation of carbonate phases. Accordingly, the decrease in the mass loss due to dehydroxylation within most samples (i.e. CS, RMC-M, HA.CS and HA.RMC-M) was an indication of the conversion of brucite to HMCs. Alternatively, the increase in the mass loss due to dehydroxylation within samples RMC-H and HA.RMC-H could be attributed to the continuation of hydration in the presence of H in these samples, which was in line with the decrease in the amount of unhydated MgO, as shown by Figs. 15 and 16. The high mass loss values corresponding to decarbonation, as shown in Tables 3 and 4, highlighted the enhanced CO_2 sequestration observed in RMC-H and HA.RMC-H samples. The higher utilisation of RMC in hydration and carbonation reactions within RMC-H formulations resulted in the highest mass loss values (~55%) amongst all samples, revealing the significant improvements in hydration and carbonation in samples RMC-H and HA.RMC-H. Along with these samples, stimulation of the carbonation process was also observed in samples involving the use of HA and/or M. Overall, sample HA.RMC-M demonstrated the highest mass loss due to decarbonation (31.5% vs. 19.5-28.5%) amongst all samples, mainly attributed to the inclusion of 40% M, which could explain its highest compressive strength under all conditions, in line with the increased formation of carbonate phases.

4. Discussion

This study focused on the development of sustainable RMC formulations involving different carbonate additives that played a key role in the enhancement of the hyration and carbonation reactions, meanwhile enabling the long term storage of CO_2 in concrete formulations. This was achieved via the use of H and M along with RMC in the presence of HA, whose synergistic

combination led to different advancements in the properties of the final products. The details of each blend (RMC-H and RMC-M) are discussed in detail below, highlighting the key points in the effective use of these additives in RMC formulations.

4.1 Effective use of H in RMC blends

The obtained results revealed the acceleration in the reaction mechanisms in the presence of H, which was evident from the increased utilisation of RMC in the hydration reaction. In addition to the enhancement of the hydration of RMC, the inclusion of H in sample RMC-H changed the morphologies of hydration products and stimulated the formation of poorly crystalline/amorphous $Mg(OH)_2$. These phases could act as an intermediate stage during the transiton of $Mg(OH)_2$ into carbonate phases [41]. Microstructural analysis reavealed the high cohesion of these phases to form large hydrate crystals in RMC-H blends (Figs. 7(b) and 8(b)), which could contribute to the strength development of these mixes [41]. Two mass loss steps corresponding to dehydration, whose peaks were at ~80°C and ~280°C, were observed in samples RMC-H and HA.RMC-H after 2 days of curing under ambient conditions (Fig. 19). Since the hydration of RMC (i.e. CS and HA.CS) did not result in any dehydration peak and the dehydration of pure H only occurred at ~280°C [59-61], the dehydration peak observed in these samples at ~80°C could correspond to bound water, which resulted in the improved morphology of hydrated phases with high cohesion, as shown in Figs. 7(b) and 8(b). Previous studies [43] hypothesised that this additional bound water represented the poorly crystalline phases in RMC-H samples. It was speculated that the presence of this bound water could have enabled the bond between $Mg(OH)_2$ and H to form a bird nest-like structure (Figs. 11 and 13), thereby reducing the crystallinity of brucite.

A further confirmation of the presence of these phases was achieved via XRD patterns (Figs. 15 and 16), which demonstrated broad brucite reflections as opposed to the usually observed sharp reflections of crystalline brucite (at 18.6°, 38.1° and 50.9° 2θ) in RMC mixes [34, 62, 63]. The disappearance of these reflections after carbonation was an indication of the propensity of these amorphous phases to carbonate, resulting in the formation of major HMC phases such as dypingite (at 8.3° 2θ) and hydromagnesite (at 15.3° 2θ). The bird nest-like structure was still present after carbonation (Figs. 12 and 14). When compared with RMC formulations presented in previous studies [10, 11, 26, 53, 54, 64, 65], these reflections of

dypingite and hydromagnesite were very obvious in RMC-H samples presented in this study (Fig. 16). The inclination of these phases to carbonate was also illustrated by the mass loss associated with decarbonation observed in samples RMC-H and HA.RMC-H after 28 days of carbonation (Tables 3 and 4), which demonstrated the largest increase in mass loss amongst all samples, despite the limited CO_2 diffusion due to the high water content present in the pores of these samples [66].

The increased hydration and carbonation reactions in these samples translated into the highest utilisation of RMC, proven by the lowest unhydrated MgO contents in samples RMC-H and HA.RMC-H after carbonation (Fig. 16). Therefore, the use of H could not only enable increased CO_2 sequestration and storage within RMC formulations via the enhanced formation of hydrate and carbonate phases, but also facilitate the effective use of RMC as a binder within concrete mixes. This resolves a key issue for the development of RMC-based concrete mixes, which had been suffering from high amounts of unhydrated/uncarbonated $MgO/Mg(OH)_2$, despite the use of various hydration and carbonation agents [10, 33, 67, 68]. One challenge that limits the strength development of RMC-H blends is their high water demand associated with the high surface area of H (43.5 m^2/g). This can be resolved via the effective use of a suitable water reducer (superplasticizer) that can enable the maintenance of high strengths without hindering the diffusion of CO_2 in RMC-H formulations [25, 43].

4.2 Effective use of M in RMC blends

The findings reported in this study highlighted the beneficial replacement of 40% RMC with M, which accelerated the hydration of RMC (Fig. 4) and improved the morphology of hydration and carbonation products under ambient (Figs. 7 and 8) and carbonation (Fig. 9) curing, respectively. The smaller surface area of M than RMC (2.3 vs. 16.3 m^2/g) also enabled slight reductions in the w/b ratio of RMC-M blends, thereby increasing the density of the final mixes. Furthermore, the presence of M in RMC formulations provided micro-aggregates (Figs. 10(c) and (d)), which led to the increased formation of carbonates phases (Tables 3 and 4). The synergistic combination of M with HA led to a higher carbonate content than all other samples. The increase in sample density facilitated by the lower water demand as well as the increased carbonate content of RMC-M blends translated into high strength gains (Fig. 6). Accordingly sample HA.RMC-M outperformed all other samples under both ambient and carbonation

curing conditions, which was supported by the densification of microstructure via the formation of carbonate phases with improved morphologies (Figs. 8 and 9).

The effective use of M in RMC formulations is not only beneficial from a performance standpoint, but also has environmental implications. Accordingly, the most common production route for RMC involves the calcination of M via the dry route, as shown in Equation 1. Through this route, the production of 1 ton of RMC requires the use of 2.1 tons of M, resulting in the emissions of 1.1 tons of CO_2. Therefore, the partial replacement (e.g. 40%) of RMC with M saves the use of ~21% M as a natural resource and reduces 40% of CO_2 emissions and energy consumption associated with the production of RMC. As M intrinsically contains CO_2 in its original form, its inclusion in concrete formulations contributes to CO_2 sequestration, without necessitating the use of any advanced technology. Therefore, RMC-M blends involving small amounts (e.g. 0.05 M) of HA could not only result in concrete samples with high mechanical performance, but also present sustainable binder alternatives to current practices for applications that do not require the use of steel reinforcement.

$$MgCO_3 \rightarrow MgO + CO_2 \quad (1)$$

Overall, the inclusion of H enhanced the hydration and carbonation reactions within RMC formulations but led to an increase in the w/b ratio. Alternatively, the use of M provided micro-aggregates that improved the mechanical performance and reduced the w/b ratio of RMC formulations. Considering their potentially synergistic effects in the presence of a suitable w/b ratio for carbonation diffusion [69], the simultaneous inclusion of H and M in the development of RMC-H-M formulations could result in samples with high CO_2 sequestration capabilities and associated performance, meanwhile maintaining a low w/b ratio and environmental impact.

5. Conclusions

This study focused on the development of RMC formulations involving hydromagnesite (H) or magnesite (M) with/without a hydration agent (HA, magnesium acetate 0.05M), which played a key role in the enhancement of the hydration and carbonation reactions and enabled increased CO_2 sequestration. The partial replacement of RMC by H and M stimulated the

increased precipitation and growth of hydrate and carbonate phases, resulting in RMC blends with improved performance and sustainability, whose details are summarized below.

The use of 20% H increased the rate and degree of the hydration reaction and resulted in additional bonding water, which formed a bond between $Mg(OH)_2$ and H. This bond led to the formation of a bird nest-like structure with poorly crystalline/amorphous brucite. The higher propensity of this amorphous phase for carbonation resulted in the enhanced formation of HMC phases such as hydromagnesite and dypingite. The presence of this bird nest-like structure was still detected after carbonation. Overall, the presence of H increased the utilization of RMC as a binder by facilitating its conversion into strength-providing HMCs in concrete mixes, whose strength could be further increased via the use of a water-reducer. Alternatively, the use of M in RMC formulations led to a significant increase in strength via the increased carbonate content and the reduction in w/b ratio of the resulting mixes. The presence of M provided micro-aggregates that facilitated the enhanced formation of dense carbonate crystals with improved morphologies, resulting in the densification of microstructure and improved performance (i.e. 113% higher strengths than CS). Furthermore, the replacement of 40% of RMC with M enabled the reduction of natural resources, CO_2 emissions and energy consumption associated with the production of RMC via the dry-route.

Overall, the results of this study highlighted the potential of RMC blends to achieve high strengths and lower environmental impacts without requiring any significant alterations of their chemistry. The synergistic combination of RMC with these additives resulted in binders with enhanced properties, enabling their use in various building applications. Future studies will look into the inclusion of additives in RMC-H-M formulations to increase their CO_2 sequestration capabilities and performance, meanwhile maintaining low w/b ratios and minimum environmental impact.

Acknowledgment

The authors would like to acknowledge the financial support from the Singapore MOE Academic Research Fund Tier 1 (RG 95/16) for the completion of this research project.

References

[1] A.L. Harrison, I.M. Power, G.M. Dipple, Accelerated Carbonation of Brucite in Mine Tailings for Carbon Sequestration, Environmental Science & Technology 47(1) (2013) 126-134.

[2] L. Mo, D.K. Panesar, Accelerated carbonation–A potential approach to sequester CO2 in cement paste containing slag and reactive MgO, Cement and Concrete Composites 43 (2013) 69-77.

[3] N. Vlasopoulos, C.R. Cheeseman, Binder composition, Google Patents, 2013.

[4] D.K. Panesar, L. Mo, Properties of binary and ternary reactive MgO mortar blends subjected to CO2 curing, Cement and Concrete Composites 38 (2013) 40-49.

[5] A.J.W. Harrison, Reactive magnesium oxide cements, Google Patents, United States of America 2008.

[6] C. Sonat, C.H. Lim, M. Liska, C. Unluer, Recycling and reuse of reactive MgO cements–A feasibility study, Construction and Building Materials 157 (2017) 172-181.

[7] G. Mármol, L. Mattoso, A.C. Correa, C.A. Fioroni, H. Savastano, Influence of cellulose pulp on the hydration followed by fast carbonation of MgO-based binders, Journal of CO2 Utilization 41 (2020) 101236.

[8] I.M. Power, G.M. Dipple, P.S. Francis, Assessing the carbon sequestration potential of magnesium oxychloride cement building materials, Cement and Concrete Composites 78 (2017) 97-107.

[9] J. Morrison, G. Jauffret, J.L. Galvez-Martos, F.P. Glasser, Magnesium-based cements for CO 2 capture and utilisation, Cement and Concrete Research 85 (2016) 183-191.

[10] R. Hay, K. Celik, Accelerated carbonation of reactive magnesium oxide cement (RMC)-based composite with supercritical carbon dioxide (scCO2), Journal of Cleaner Production 248 (2020) 119282.

[11] L.J. Vandeperre, A. Al-Tabbaa, Accelerated carbonation of reactive MgO cements, Advances in Cement Research 19(2) (2007) 67-79.

[12] N.T. Dung, T.J.N. Hooper, C. Unluer, Enhancing the performance of MgO-activated slag-fly ash mixes by accelerated carbonation, Journal of CO2 Utilization 42 (2020) 101356.

[13] R. Zhang, N. Bassim, D.K. Panesar, Characterization of Mg components in reactive MgO – Portland cement blends during hydration and carbonation, Journal of CO2 Utilization 27 (2018) 518-527.

[14] V.S.S. Birchal, S.D.F. Rocha, V.S.T. Ciminelli, The effect of magnesite calcination conditions on magnesia hydration, Minerals Engineering 13(14–15) (2000) 1629-1633.

[15] K. Hirota, N. Okabayashi, K. Toyoda, O. Yamaguchi, Characterization and sintering of reactive MgO, Materials Research Bulletin 27(3) (1992) 319-326.

[16] L. Mo, M. Deng, M. Tang, Effects of calcination condition on expansion property of MgO-type expansive agent used in cement-based materials, Cement and Concrete Research 40(3) (2010) 437-446.

[17] F.C. Harper, Effect of calcination temperature on the properties of magnesium oxides for use in magnesium oxychloride cements, Journal of Applied Chemistry 17(1) (1967) 5-10.

[18] H. Dong, E.-H. Yang, C. Unluer, F. Jin, A. Al-Tabbaa, Investigation of the properties of MgO recovered from reject brine obtained from desalination plants, Journal of Cleaner Production 196 (2018) 100-108.

[19] J. Green, Calcination of precipitated Mg(OH)2 to active MgO in the production of refractory and chemical grade MgO, Journal of Materials Science 18(3) (1983) 637-651.

[20] W.R. Eubank, Calcination Studies of Magnesium Oxides, Journal of the American Ceramic Society 34(8) (1951) 225-229.

[21] H. Dong, C. Unluer, E.-H. Yang, A. Al-Tabbaa, Recovery of reactive MgO from reject brine via the addition of NaOH, Desalination 429 (2018) 88-95.

[22] J.J. Thomas, S. Musso, I. Prestini, Kinetics and activation energy of magnesium oxide hydration, Journal of the American Ceramic Society 97(1) (2014) 275-282.

[23] X. Tang, L. Guo, C. Chen, Q. Liu, T. Li, Y. Zhu, The analysis of magnesium oxide hydration in three-phase reaction system, Journal of Solid State Chemistry 213 (2014) 32-37.

[24] N.T. Dung, C. Unluer, Carbonated MgO concrete with improved performance: The influence of temperature and hydration agent on hydration, carbonation and strength gain, Cement and Concrete Composites 82 (2017) 152-164.

[25] N.T. Dung, C. Unluer, Improving the performance of reactive MgO cement-based concrete mixes, Construction and Building Materials 126 (2016) 747-758.

[26] M. Liska, A. Al-Tabbaa, K. Carter, J. Fifield, Scaled-up commercial production of reactive magnesia cement pressed masonry units. Part II: Performance, Proceedings of the Institution of Civil Engineers-Construction Materials 165(4) (2012) 225-243.

[27] M. Liska, L.J. Vandeperre, A. Al-Tabbaa, Influence of carbonation on the properties of reactive magnesia cement-based pressed masonry units, Advances in cement research 20(2) (2008) 53-64.

[28] N.T. Dung, C. Unluer, Influence of accelerated hydration and carbonation on the performance of reactive magnesium oxide concrete, Advances in Cement Research (2018) 1-13.

[29] L. Wang, L. Chen, J.L. Provis, D.C.W. Tsang, C.S. Poon, Accelerated carbonation of reactive MgO and Portland cement blends under flowing CO2 gas, Cement and Concrete Composites 106 (2020) 103489.

[30] S. Ma, A.H. Akca, D. Esposito, S. Kawashima, Influence of aqueous carbonate species on hydration and carbonation of reactive MgO cement, Journal of CO2 Utilization 41 (2020) 101260.

[31] N.T. Dung, C. Unluer, Sequestration of CO2 in reactive MgO cement-based mixes with enhanced hydration mechanisms, Construction and Building Materials 143 (2017) 71-82.

[32] N.T. Dung, C. Unluer, Performance of reactive MgO concrete under increased CO2 dissolution, Cement and Concrete Research 118 (2019) 92-101.

[33] N.T. Dung, C. Unluer, Development of MgO concrete with enhanced hydration and carbonation mechanisms, Cement and Concrete Research 103 (2018) 160-169.

[34] N.T. Dung, A. Lesimple, R. Hay, K. Celik, C. Unluer, Formation of carbonate phases and their effect on the performance of reactive MgO cement formulations, Cement and Concrete Research 125 (2019) 105894.

[35] L. Chen, L. Wang, D.C.W. Tsang, V. Mechtcherine, C.S. Poon, Efficacy of green alternatives and carbon dioxide curing in reactive magnesia cement-bonded particleboards, Journal of Cleaner Production 258 (2020) 120997.

[36] A. Khalil, X. Wang, K. Celik, 3D printable magnesium oxide concrete: towards sustainable modern architecture, Additive Manufacturing 33 (2020) 101145.

[37] N.T. Dung, R. Hay, A. Lesimple, K. Celik, C. Unluer, Influence of CO2 concentration on the performance of MgO cement mixes, Cement and Concrete Composites 115 (2021) 103826.

[38] R. Zhang, D.K. Panesar, Water absorption of carbonated reactive MgO concrete and its correlation with the pore structure, Journal of CO2 Utilization 24 (2018) 350-360.

[39] R.J. Flatt, N. Roussel, C.R. Cheeseman, Concrete: An eco material that needs to be improved, Journal of the European Ceramic Society 32(11) (2012) 2787-2798.

[40] M. Achternbosch, C. Kupsch, E. Nieke, G. Sardemann, Are new magnesia-based cements the future? Part 1: Analysis of former developments, ZKG INTERNATIONAL 65 (2012) 64-72.

[41] C. Kuenzel, F. Zhang, V. Ferrándiz-Mas, C.R. Cheeseman, E.M. Gartner, The mechanism of hydration of MgO-hydromagnesite blends, Cement and Concrete Research 103 (2018) 123-129.

[42] M. Achternbosch, C. Kupsch, E. Nieke, G. Sardemann, Are new magnesia-based cements the future? Part 2: Novacem - An assessment of new developments, ZKG INTERNATIONAL 65 (2012) 64-72.

[43] F. Winnefeld, E. Epifania, F. Montagnaro, E.M. Gartner, Further studies of the hydration of MgO-hydromagnesite blends, Cement and Concrete Research 126 (2019) 105912.

[44] N.T. Dung, C. Unluer, Advances in the hydration of reactive MgO cement blends incorporating different magnesium carbonates, Construction and Building Materials 294 (2021) 123573.

[45] E. Gartner, T. Sui, Alternative cement clinkers, Cement and Concrete Research 114 (2018) 27-39.

[46] B. Garcia, V. Beaumont, E. Perfetti, V. Rouchon, D. Blanchet, P. Oger, G. Dromart, A.Y. Huc, F. Haeseler, Experiments and geochemical modelling of CO2 sequestration by olivine: Potential, quantification, Applied Geochemistry 25(9) (2010) 1383-1396.

[47] A. Sanna, M. Uibu, G. Caramanna, R. Kuusik, M.M. Maroto-Valer, A review of mineral carbonation technologies to sequester CO2, Chemical Society Reviews 43(23) (2014) 8049-8080.

[48] E. Gartner, H. Hirao, A review of alternative approaches to the reduction of CO2 emissions associated with the manufacture of the binder phase in concrete, Cement and Concrete Research 78, Part A (2015) 126-142.

[49] ASTM C1702 − 15a, Standard test method for measurement of heat of hydration of hydraulic cementitious materials using isothermal conduction calorimetry, ASTM Committee C01, West Conshohocken, PA 19428-2959, United States, 2015, p. 8.

[50] N.C. Collier, J.H. Sharp, N.B. Milestone, J. Hill, I.H. Godfrey, The influence of water removal techniques on the composition and microstructure of hardened cement pastes, Cement and Concrete Research 38(6) (2008) 737-744.

[51] N.T. Dung, T.J.N. Hooper, C. Unluer, Accelerating the reaction kinetics and improving the performance of Na2CO3-activated GGBS mixes, Cement and Concrete Research 126 (2019) 105927.

[52] B.S.I, BS EN 771-3:2011 Specification for masonry units, Aggregate concrete masonry units (dense and lightweight aggregates).

[53] C. Unluer, A. Al-Tabbaa, Impact of hydrated magnesium carbonate additives on the carbonation of reactive MgO cements, Cement and Concrete Research 54 (2013) 87-97.

[54] C. Unluer, A. Al-Tabbaa, Enhancing the carbonation of MgO cement porous blocks through improved curing conditions, Cement and Concrete Research 59 (2014) 55-65.

[55] M. Giampouras, J.M. Garcia-Ruiz, C.J. Garrido, Crystallization Experiments in the MgO-CO2-H2O system: Role of Amorphous Magnesium Carbonate Precursors in Magnesium Carbonate Hydrated Phases and Morphologies in Low Temperature Hydrothermal Fluids, 2017, p. 14211.

[56] Y. Wang, J. Liu, T. Shi, B. Yang, C. Li, H. Xu, W. Yin, Preparation, properties and phase transition of mesoporous hydromagnesite with various morphologies from natural magnesite, Powder Technology 364 (2020) 822-830.

[57] M. Sanchez-Roman, C.S. Romanek, H. Xu, M. Coleman, Ca and Mg Incorporation in Siderite at Low Temperatures (< 50° C): Results from Laboratory Experiments, 2008, pp. P51A-1403.

[58] A.M. Chaka, Ab Initio Thermodynamics and the Relationship between Octahedral Distortion, Lattice Structure, and Proton Substitution Defects in Malachite/Rosasite Group Endmember Pokrovskite Mg2CO3(OH)2, The Journal of Physical Chemistry A 120(51) (2016) 10181-10195.

[59] L.A. Hollingbery, T.R. Hull, The thermal decomposition of huntite and hydromagnesite—A review, Thermochimica Acta 509(1–2) (2010) 1-11.

[60] Y. Sawada, K. Uematsu, N. Mizutani, M. Kato, Thermal decomposition of hydromagnesite 4MgCO3 - Mg(OH)2 - 4H2O under different partial pressures of carbon dioxide, Thermochimica Acta 27(1) (1978) 45-59.

[61] Y. Sawada, K. Uematsu, N. Mizutani, M. Kato, Thermal decomposition of hydromagnesite 4MgCO3·Mg(OH)2·4H2O, Journal of Inorganic and Nuclear Chemistry 40(6) (1978) 979-982.

[62] A.V. Saetta, B.A. Schrefler, R.V. Vitaliani, 2 — D model for carbonation and moisture/heat flow in porous materials, Cement and Concrete Research 25(8) (1995) 1703-1712.

[63] J. Fagerlund, J. Highfield, R. Zevenhoven, Kinetics studies on wet and dry gas–solid carbonation of MgO and Mg(OH)2 for CO2 sequestration, RSC Advances 2(27) (2012) 10380-10393.

[64] L.J. Vandeperre, M. Liska, A. Al-Tabbaa, Microstructures of reactive magnesia cement blends, Cement and Concrete Composites 30(8) (2008) 706-714.

[65] M. Liska, A. Al-Tabbaa, Ultra-green construction: reactive magnesia masonry products, Waste and Resource Management 162 (2008) 185-196.

[66] M. Fernández Bertos, S.J.R. Simons, C.D. Hills, P.J. Carey, A review of accelerated carbonation technology in the treatment of cement-based materials and sequestration of CO2, Journal of Hazardous Materials 112(3) (2004) 193-205.

[67] R. Hay, K. Celik, Hydration, carbonation, strength development and corrosion resistance of reactive MgO cement-based composites, Cement and Concrete Research 128 (2020) 105941.

[68] N.T. Dung, C. Unluer, Improving the Carbonation of Reactive MgO Cement Concrete via the Use of NaHCO3 and NaCl, Journal of Materials in Civil Engineering 30(12) (2018) 04018320.

[69] T. Wang, H. Huang, X. Hu, M. Fang, Z. Luo, R. Guo, Accelerated mineral carbonation curing of cement paste for CO2 sequestration and enhanced properties of blended calcium silicate, Chemical Engineering Journal 323 (2017) 320-329.

List of Tables

Table 1. Chemical composition and physical properties of RMC.

	Chemical composition (%)							Physical properties	
	MgO	SiO_2	CaO	R_2O_3	K_2O	Na_2O	LOI	Specific gravity (g/cm^3)	Specific surface area (m^2/g)
RMC	>91.5	2.0	1.6	1.0	-	-	4.0	3.0	16.3

Table 2. Mixture compositions of concrete samples used in this study.

Mix	Binder composition (%)				Mixture proportion (kg/m^3)					
	w/b	RMC	H	M	RMC	H	M	Water	HA	Aggregrates
CS	0.6	100	0	0	600	-	-	360	0	1120
RMC-H	1.2	80	20	0	480	120	-	720	0	165
RMC-M	0.55	60	0	40	360	-	240	330	0	1190
HA.CS	0.6	100	0	0	1050	-	-	360	3.6	1115
HA.RMC-H	1.2	80	20	0	472	118	-	720	7.7	157
HA.RMC-M	0.55	60	0	40	444	-	666	330	3.5	1185

Table 3. Mass loss values at different decomposition steps of samples subjected to ambient curing conditions for 2 days, obtained by TGA.

Mix	Mass loss (wt.%)			
	Dehydration	Dehydroxylation	Decarbonation	Total
CS	0.7	11.4	13.4	25.5
RMC-H	4.7	10.3	15.4	30.4
RMC-M	0.9	8.3	26.6	35.8
HA.CS	1.6	11.8	14.6	28.0
HA.RMC-H	6.0	11.3	18.2	35.5
HA.RMC-M	1.3	7.2	28.2	36.7

Table 4. Mass loss values at different decomposition steps of samples subjected to ambient curing conditions for 2 days, followed by accelerated carbonation conditions for 26 days, obtained by TGA.

Mix	Mass loss (wt.%)			
	Dehydration	Dehydroxylation	Decarbonation	Total
CS	3.2	6.2	19.5	28.8
RMC-H	15.2	15.3	24.2	54.6
RMC-M	4.1	8.1	28.5	40.7
HA.CS	3.6	6.2	21.1	30.9
HA.RMC-H	16.1	12.3	25.9	54.3
HA.RMC-M	5.9	6.7	31.5	44.1

List of Figures

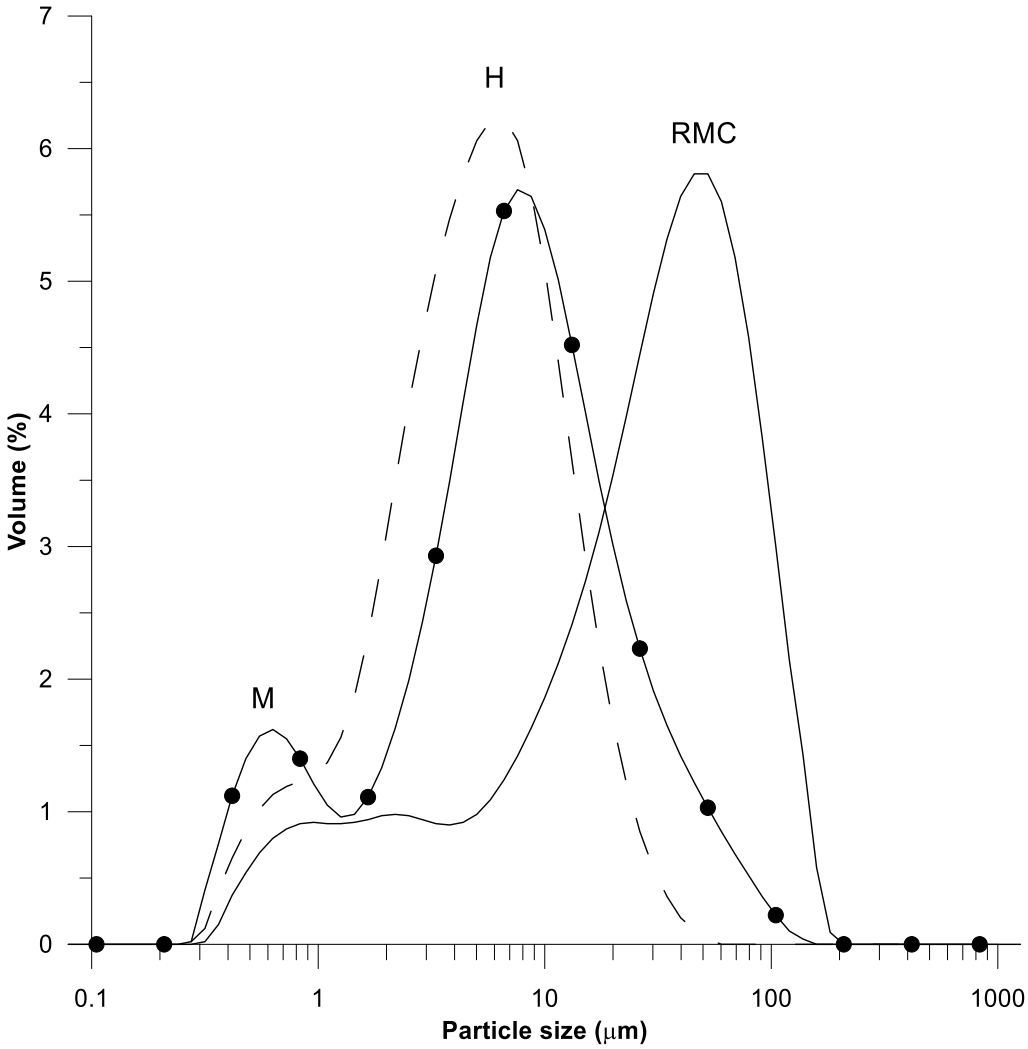

Fig. 1. Particle size distributions of RMC, H and M

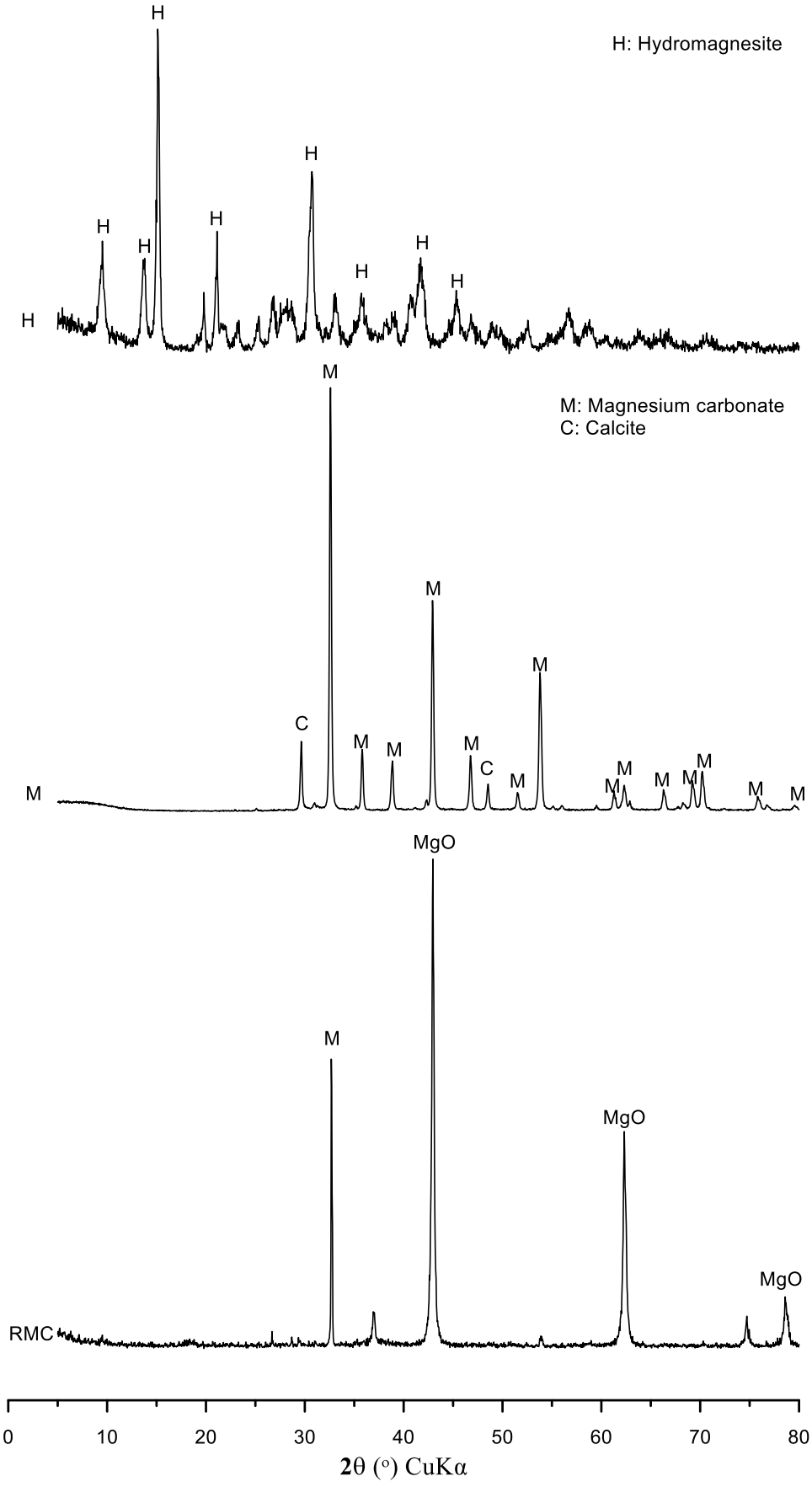

Fig. 2. XRD patterns of RMC, H and M

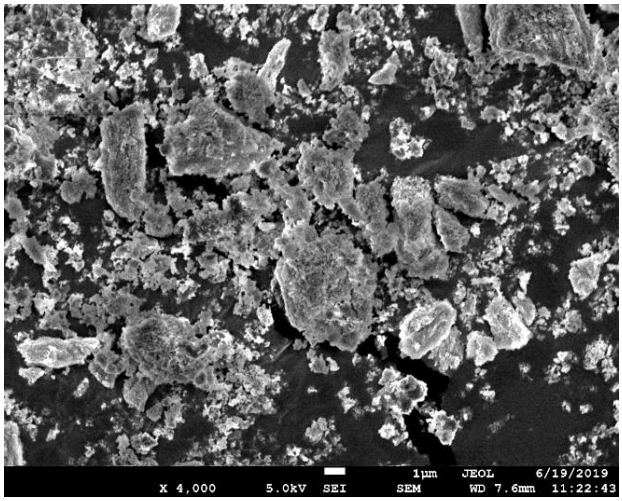

(a)

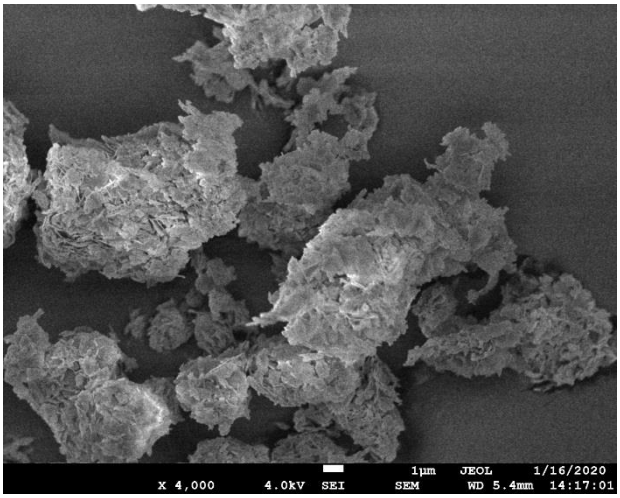

(b)

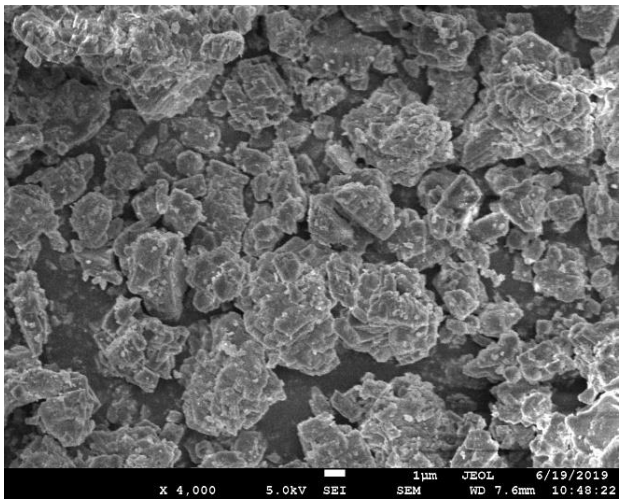

(c)

Fig. 3. Morphologies of (a) RMC, (b) H and (c) M

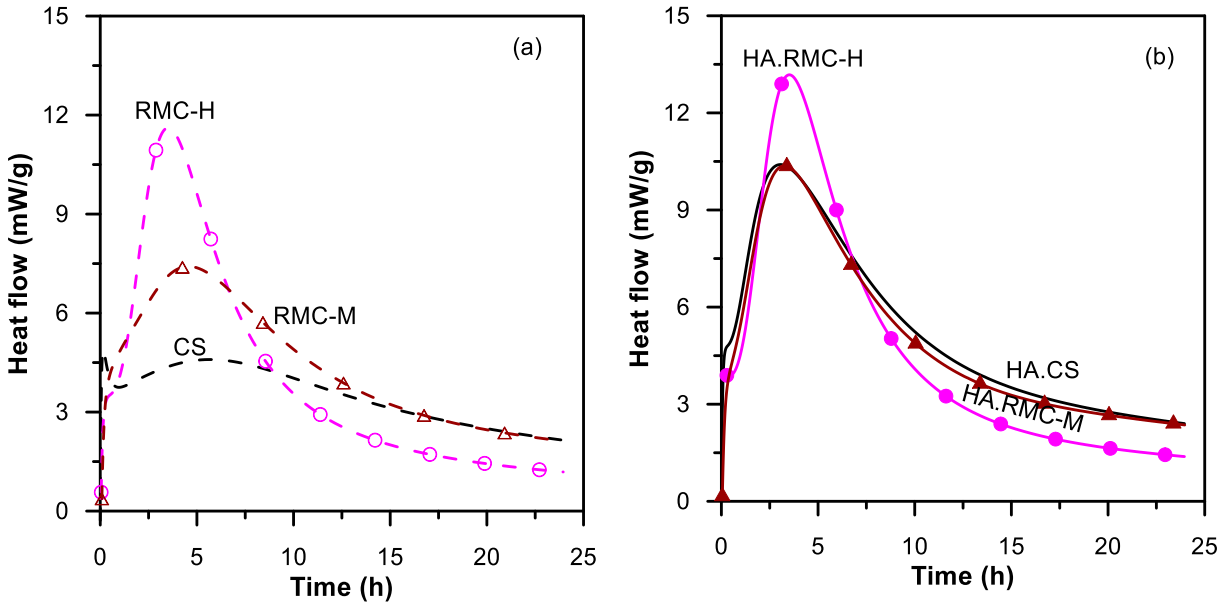

Fig. 4. Heat flow of samples (a) CS, RMC-H and RMC-M; and (b) HA.CS, HA.RMC-H and HA.RMC-M

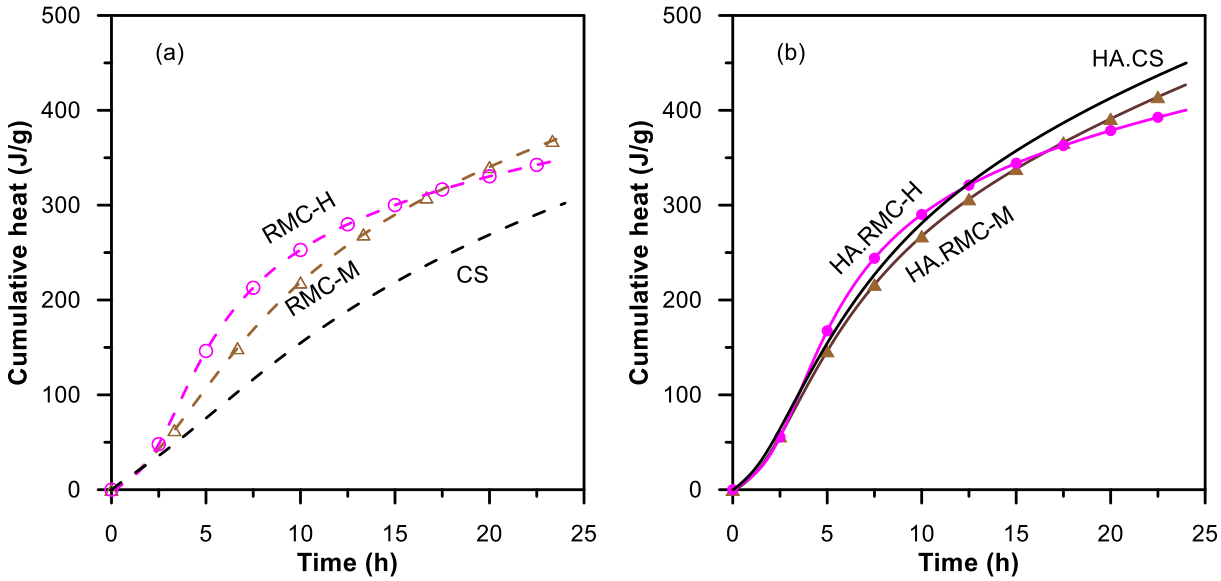

Fig. 5. Cumulative heat of samples (a) CS, RMC-H and RMC-M; and (b) HA.CS, HA.RMC-H and HA.RMC-M

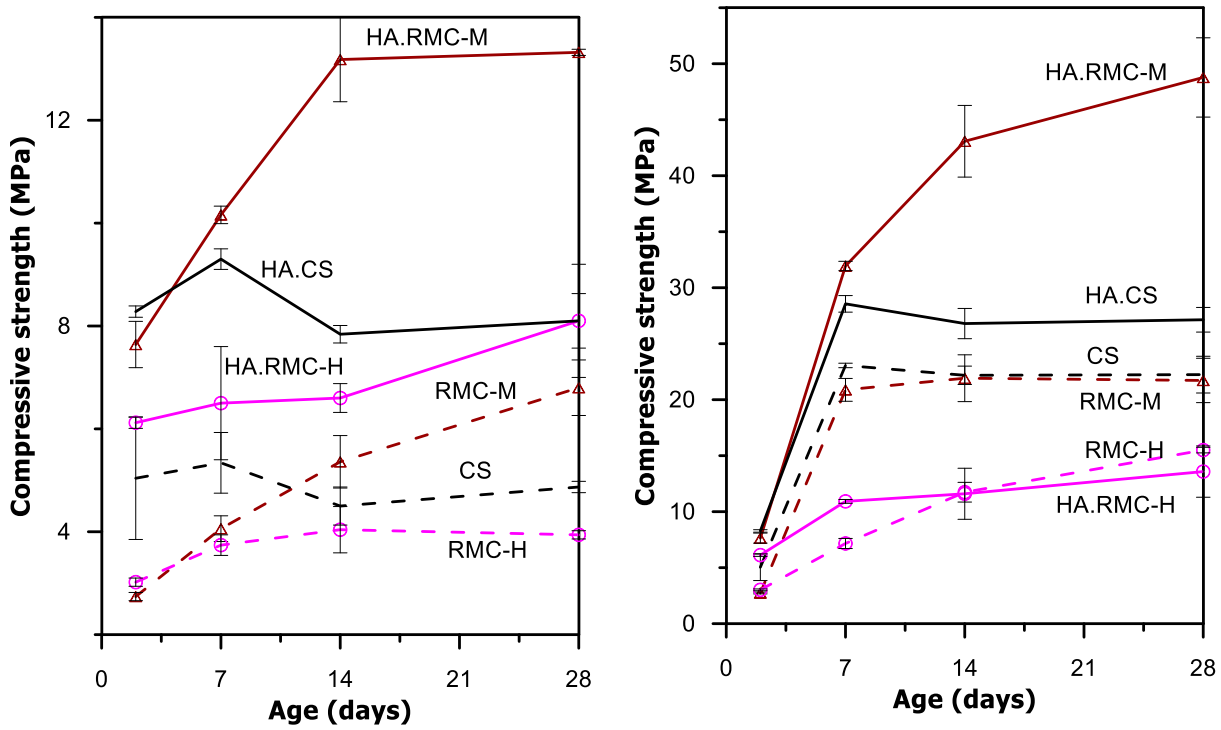

Fig. 6. Compressive strength of concrete samples cured under: (a) ambient conditions for 28 days and (b) ambient conditions for 2 days, followed by accelerated carbonation conditions for 26 days

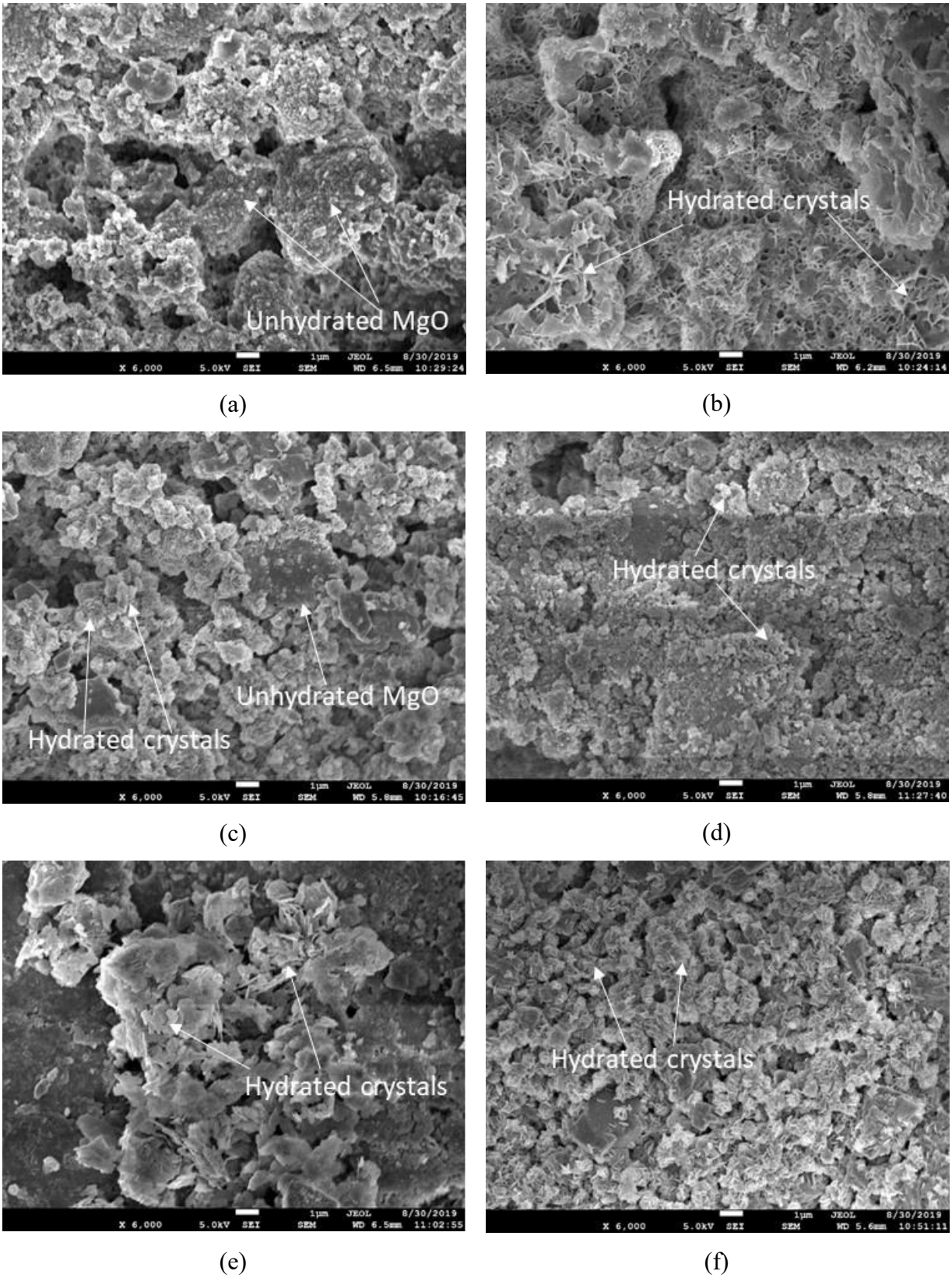

Fig. 7. SEM images of samples cured under ambient conditions for 2 days: (a) CS, (b) RMC-H, (c) RMC-M, (d) HA.CS, (e) HA.RMC-H and (f) HA.RMC-M

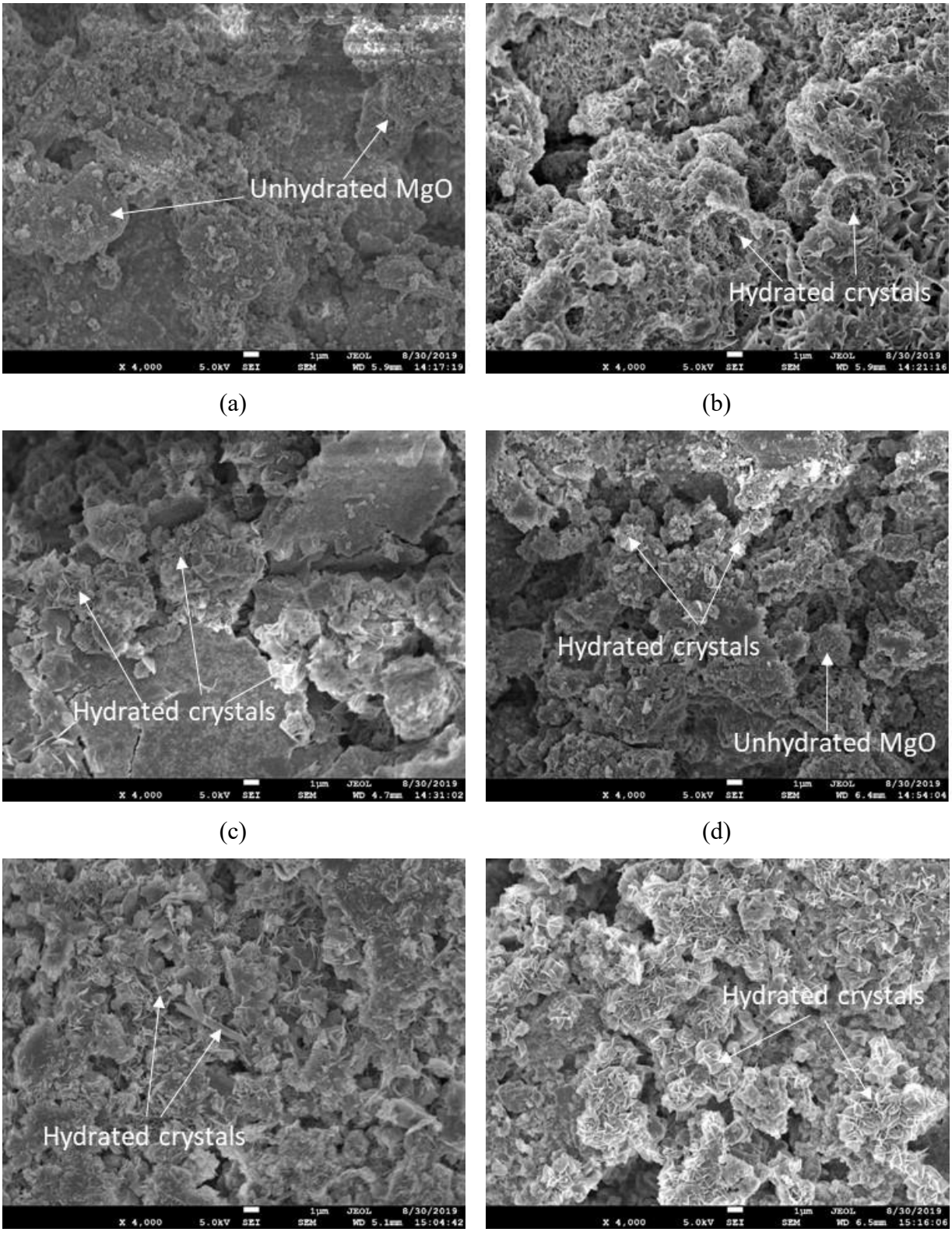

Fig. 8. SEM images of samples cured under ambient conditions for 28 days: (a) CS, (b) RMC-H, (c) RMC-M, (d) HA.CS, (e) HA.RMC-H and (f) HA.RMC-M

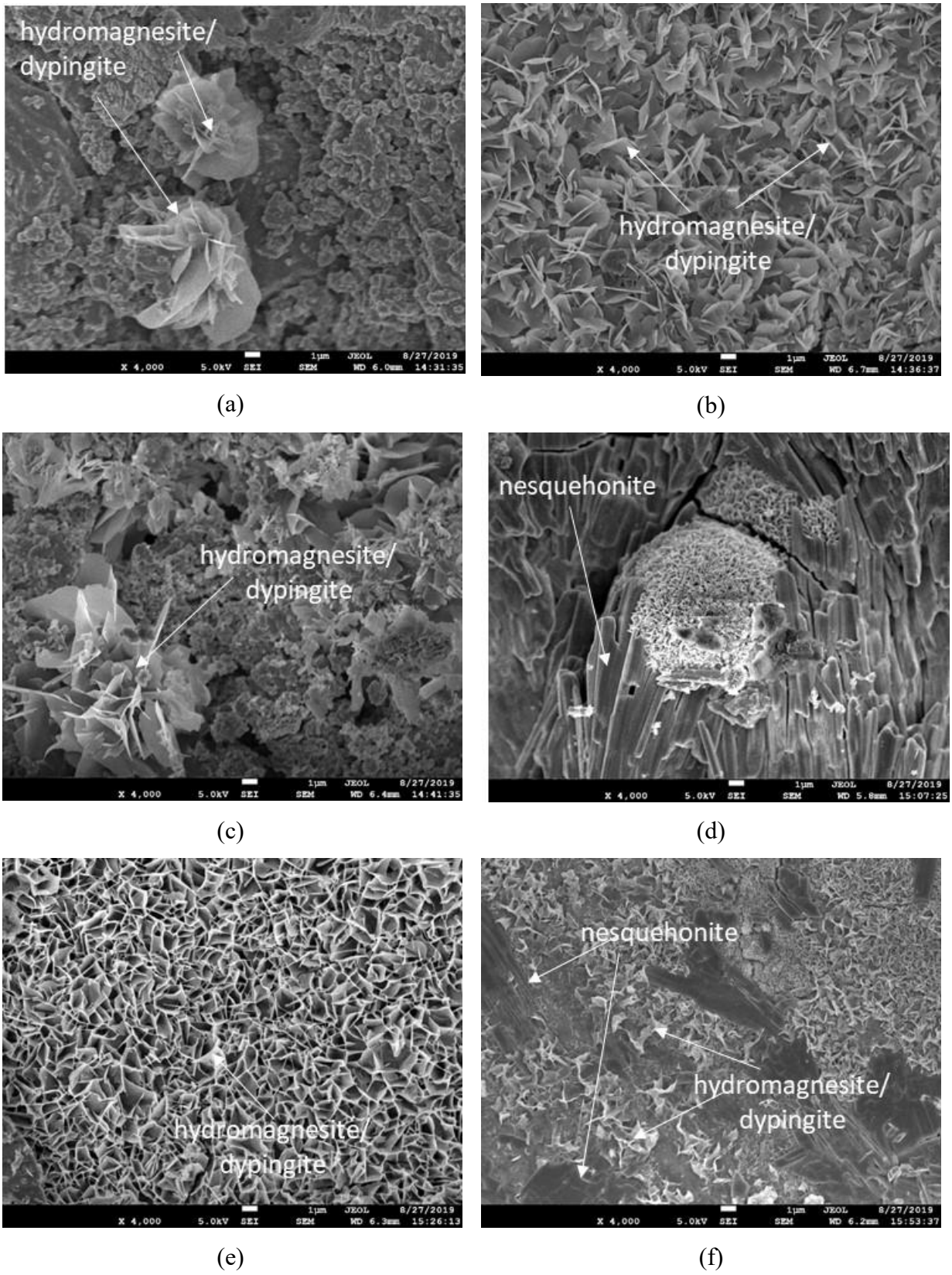

Fig. 9. SEM images of samples cured under ambient conditions for 2 days, followed by accelerated carbonation conditions for 26 days: (a) CS, (b) RMC-H, (c) RMC-M, (d) HA.CS, (e) HA.RMC-H and (f) HA.RMC-M

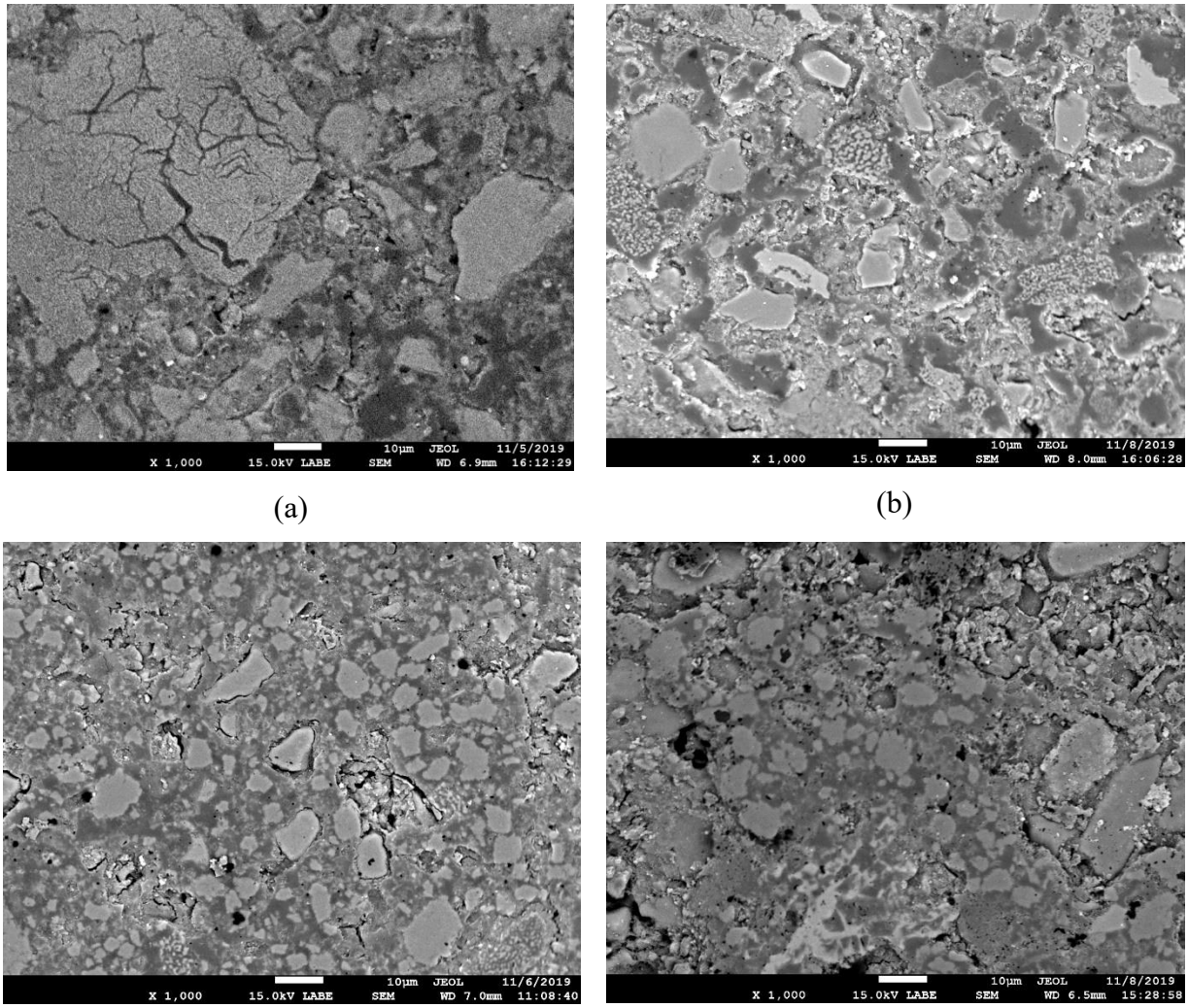

Fig. 10. BSE images of carbonated samples at 28 days: (a) CS, (b) HA.CS, (c) RMC-M and (d) HA.RMC-M

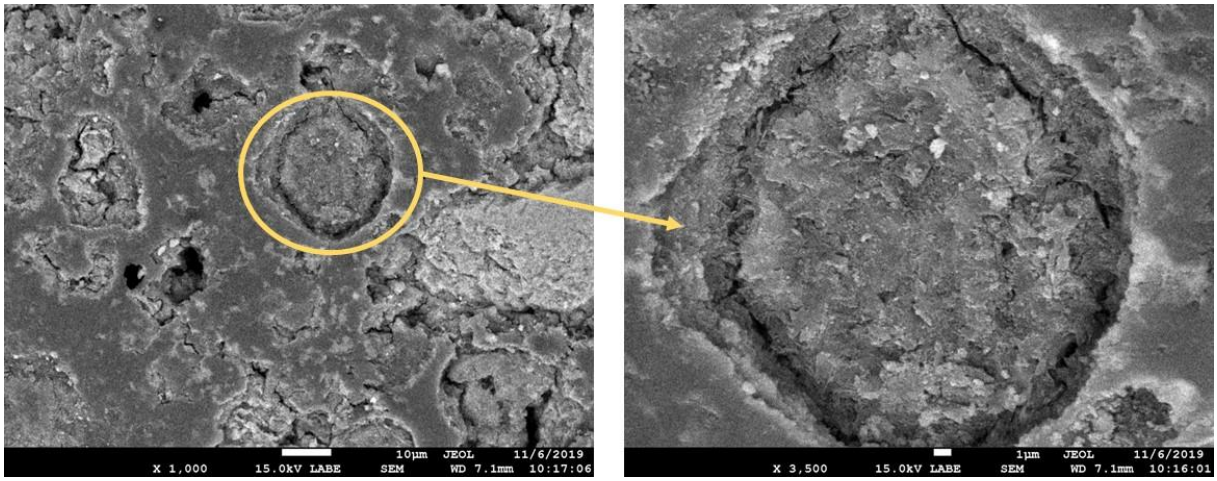

Fig. 11. BSE images of carbonated sample RMC-H at 28 days

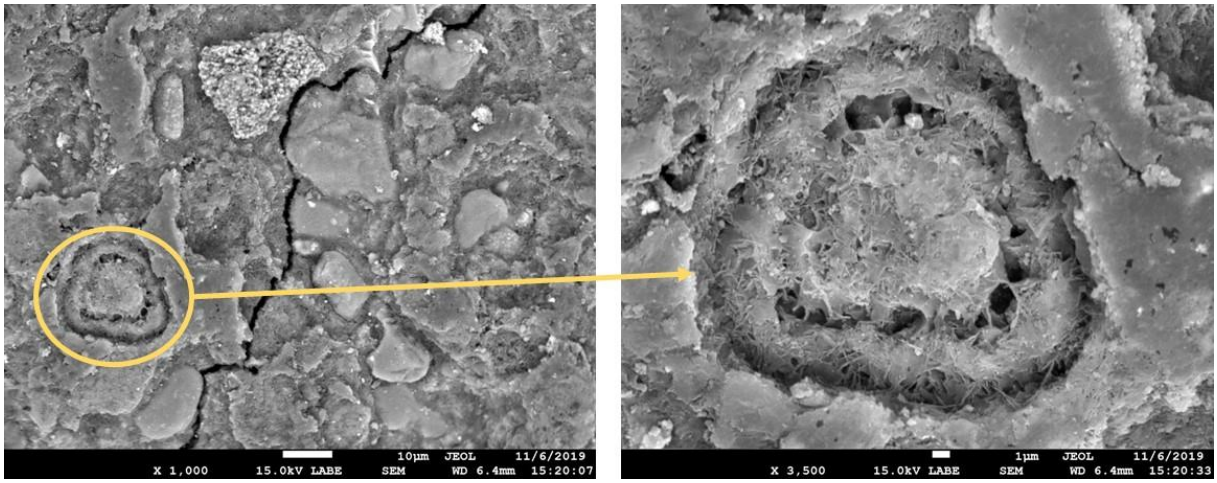

Fig. 12. BSE images of carbonated sample HA.RMC-H at 28 days

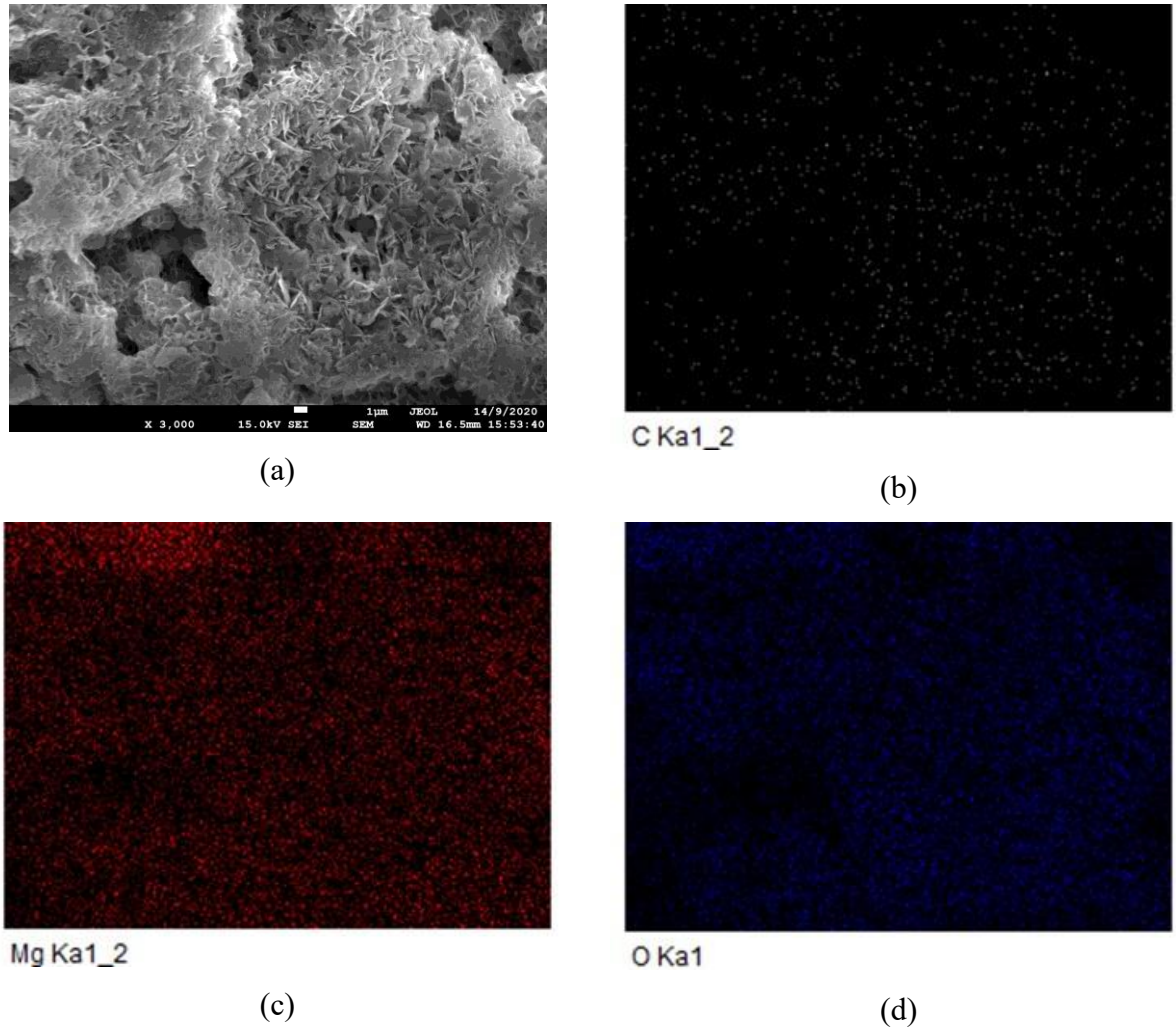

(a) (b) (c) (d)

Fig. 13. Microstructural analysis of the bird nest-like structure within samples cured under ambient conditions for 2 days: (a) SEM image, and EDX results showing: (b) distribution of C, (c) distribution of M, and (d) distribution of O

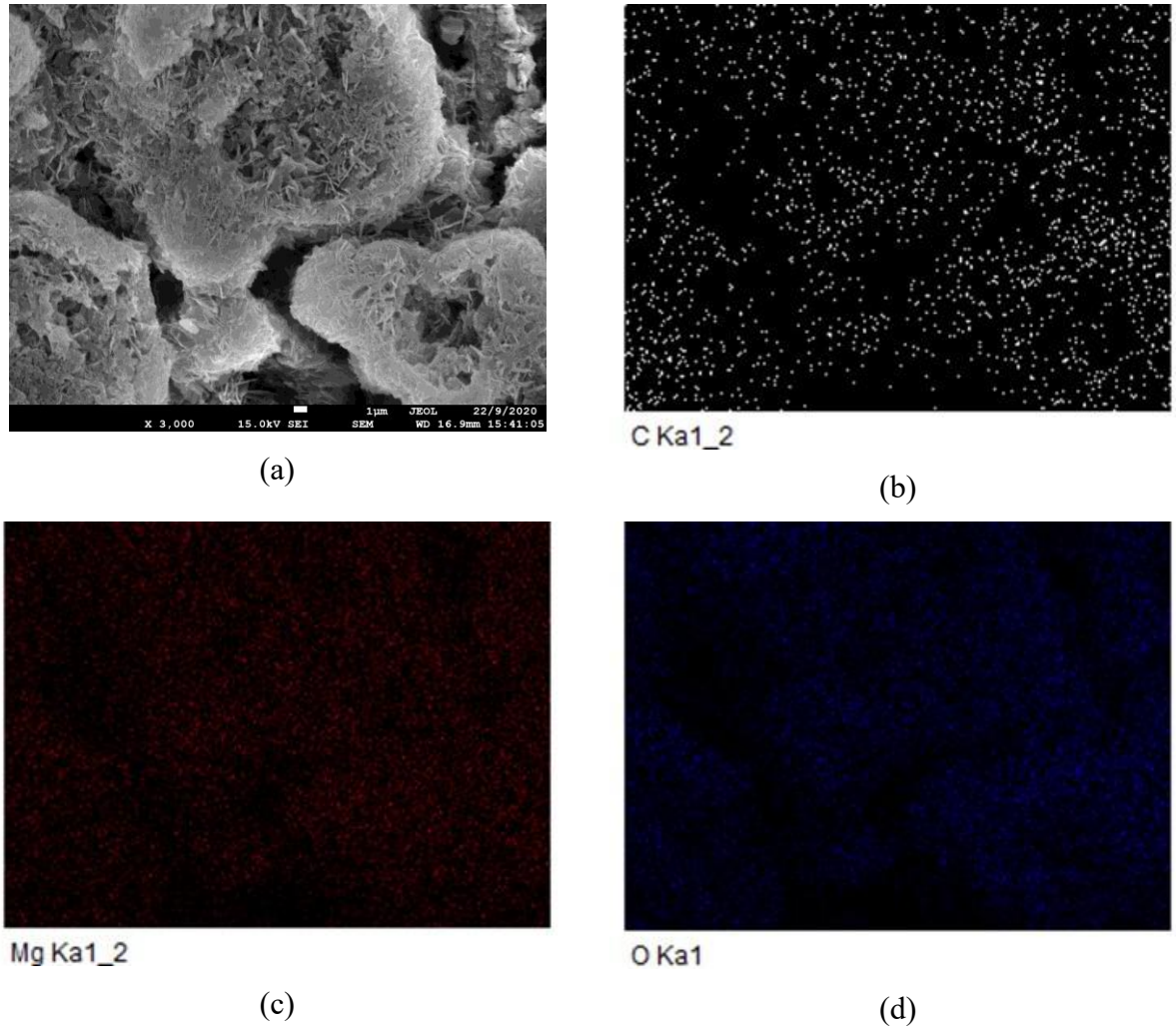

(a) (b) (c) (d)

Fig. 14. Microstructural analysis of the bird nest-like structure within samples cured under accelerated carbonation conditions for 7 days: (a) SEM image, and EDX results showing: (b) distribution of C, (c) distribution of M, and (d) distribution of O

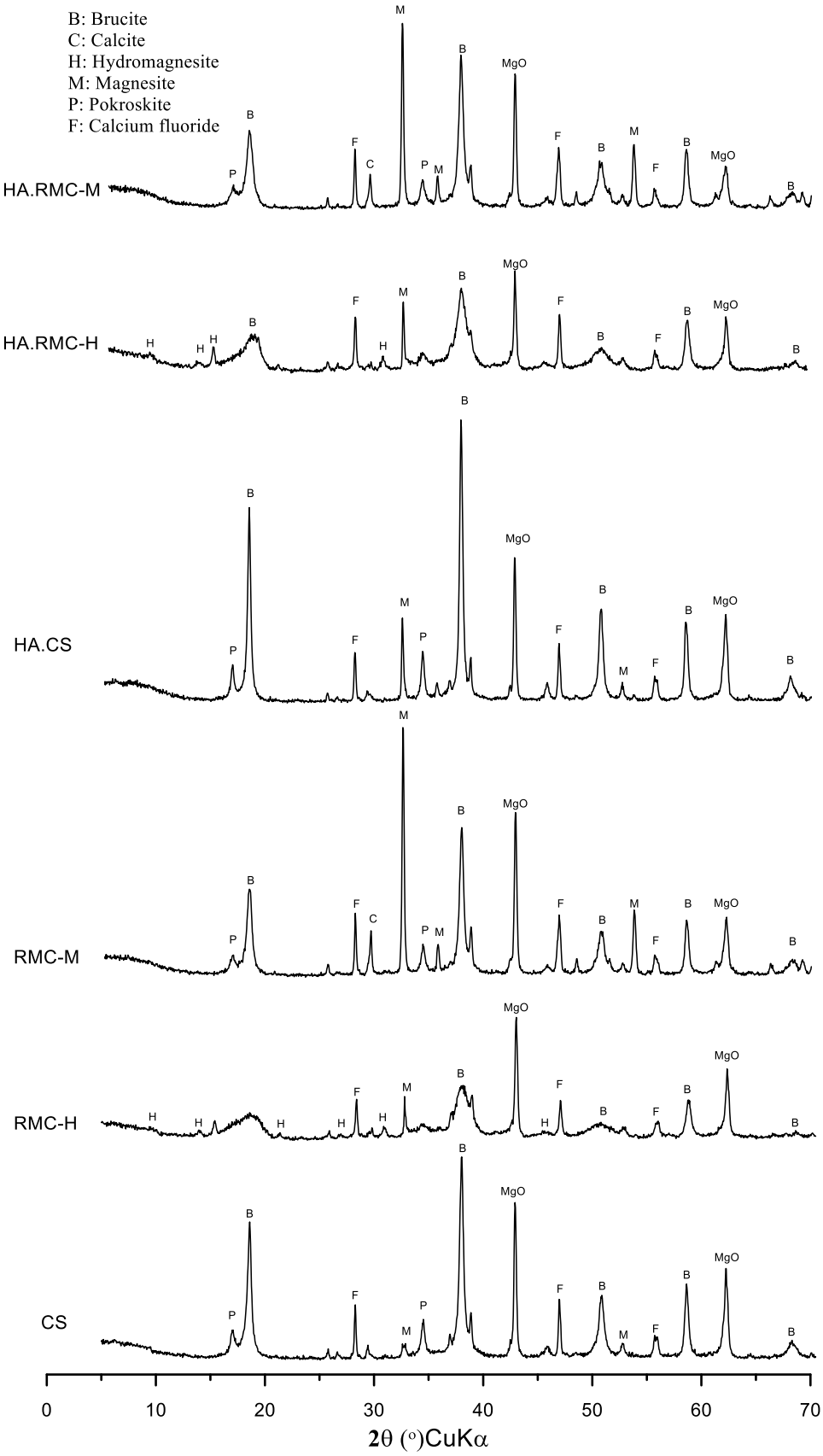

Fig. 15. XRD patterns of concrete samples cured under ambient conditions for 2 days

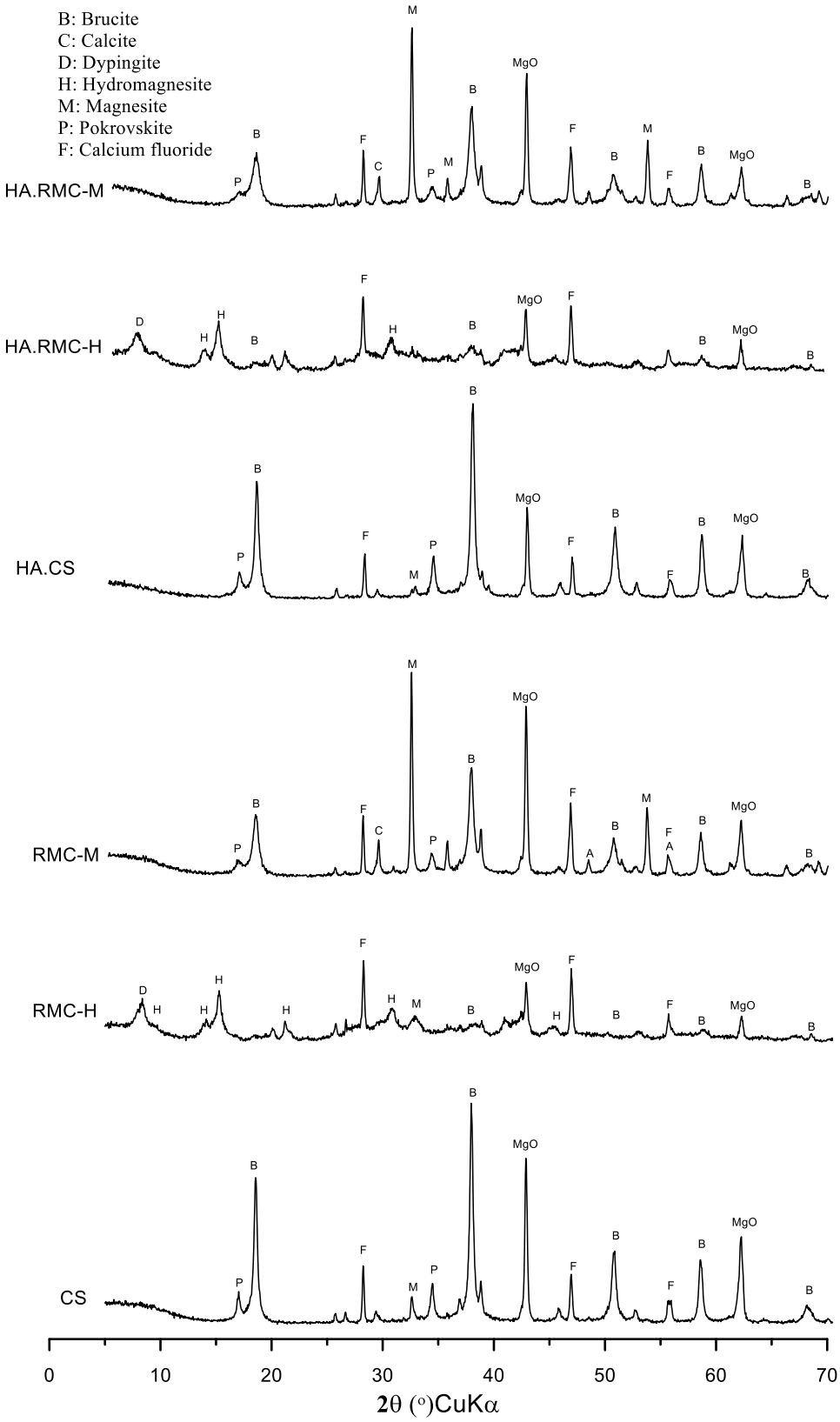

Fig. 16. XRD patterns of concrete samples cured under ambient conditions for 2 days, followed by 26 days of accelerated carbonation conditions

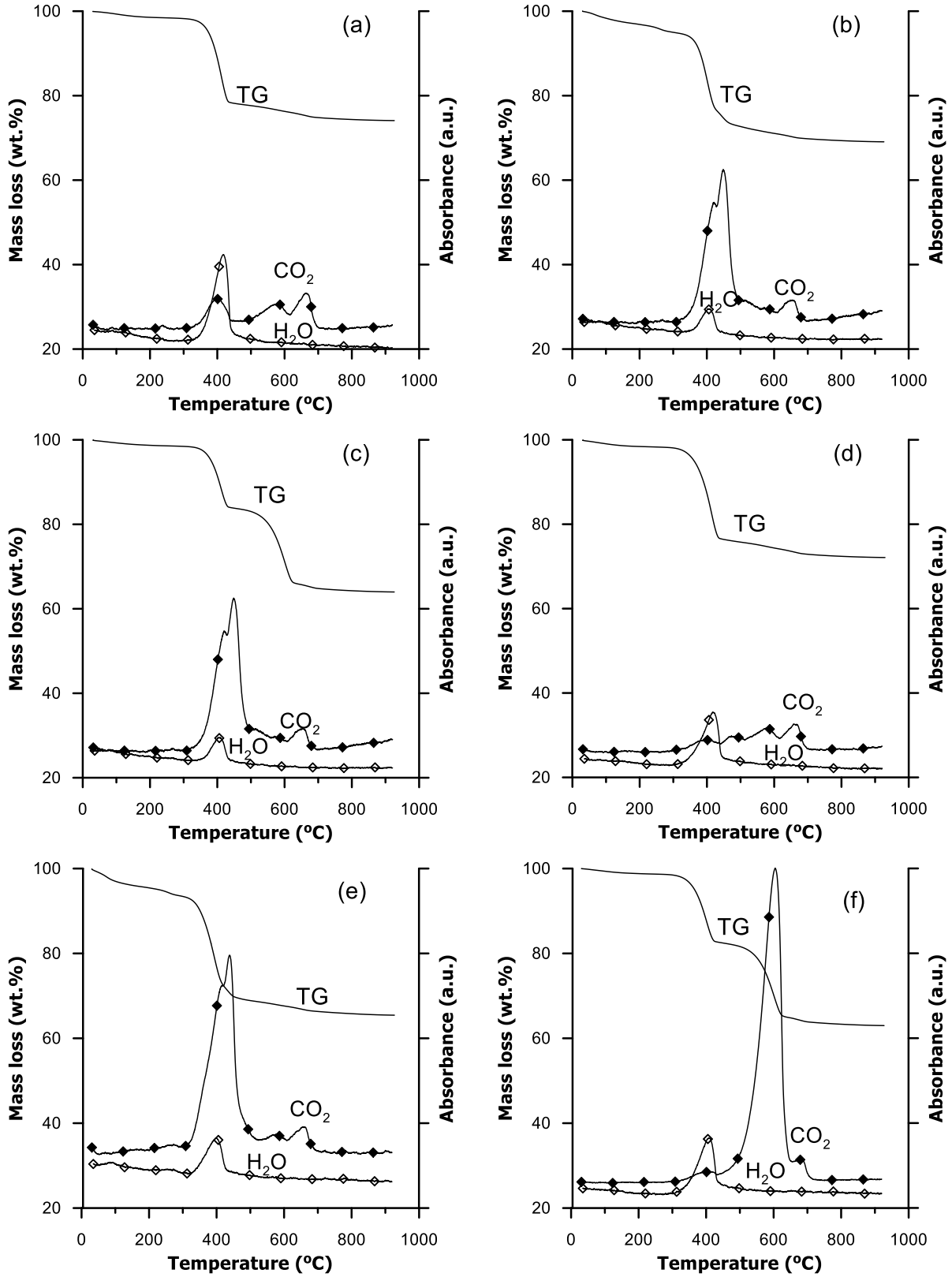

Fig. 17. TG-IR results of samples cured under ambient conditions for 2 days: (a) CS, (b) RMC-H, (c) RMC-M, (d) HA.CS, (e) HA.RMC-H and (f) HA.RMC-M

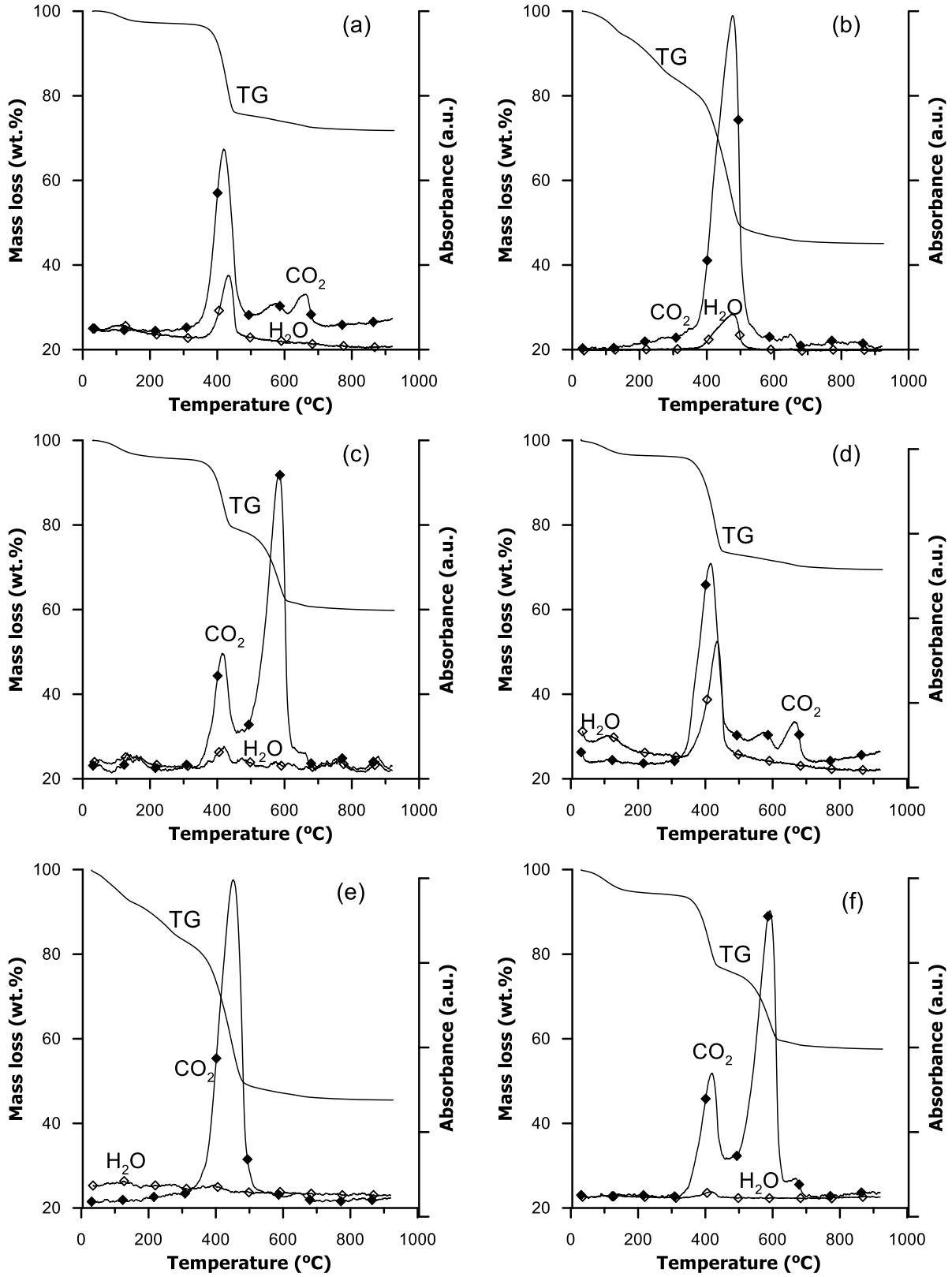

Fig. 18. TG-IR results of samples cured under ambient conditions for 2 days, followed by accelerated carbonation conditions for 26 days: (a) CS, (b) RMC-H, (c) RMC-M, (d) HA.CS, (e) HA.RMC-H and (f) HA.RMC-M

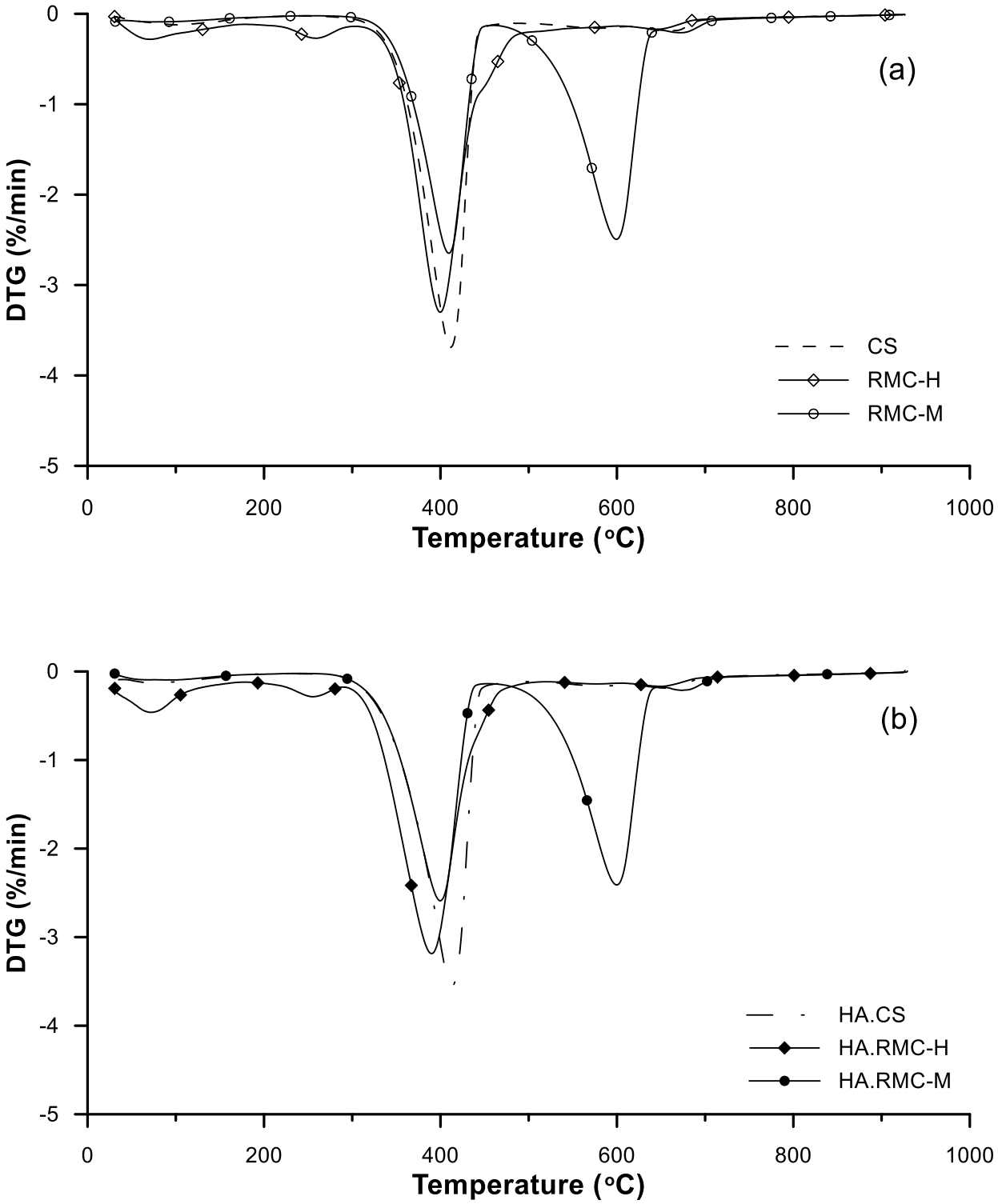

Fig. 19. DTG curves of samples cured under ambient conditions for 2 days: (a) without HA and (b) with HA

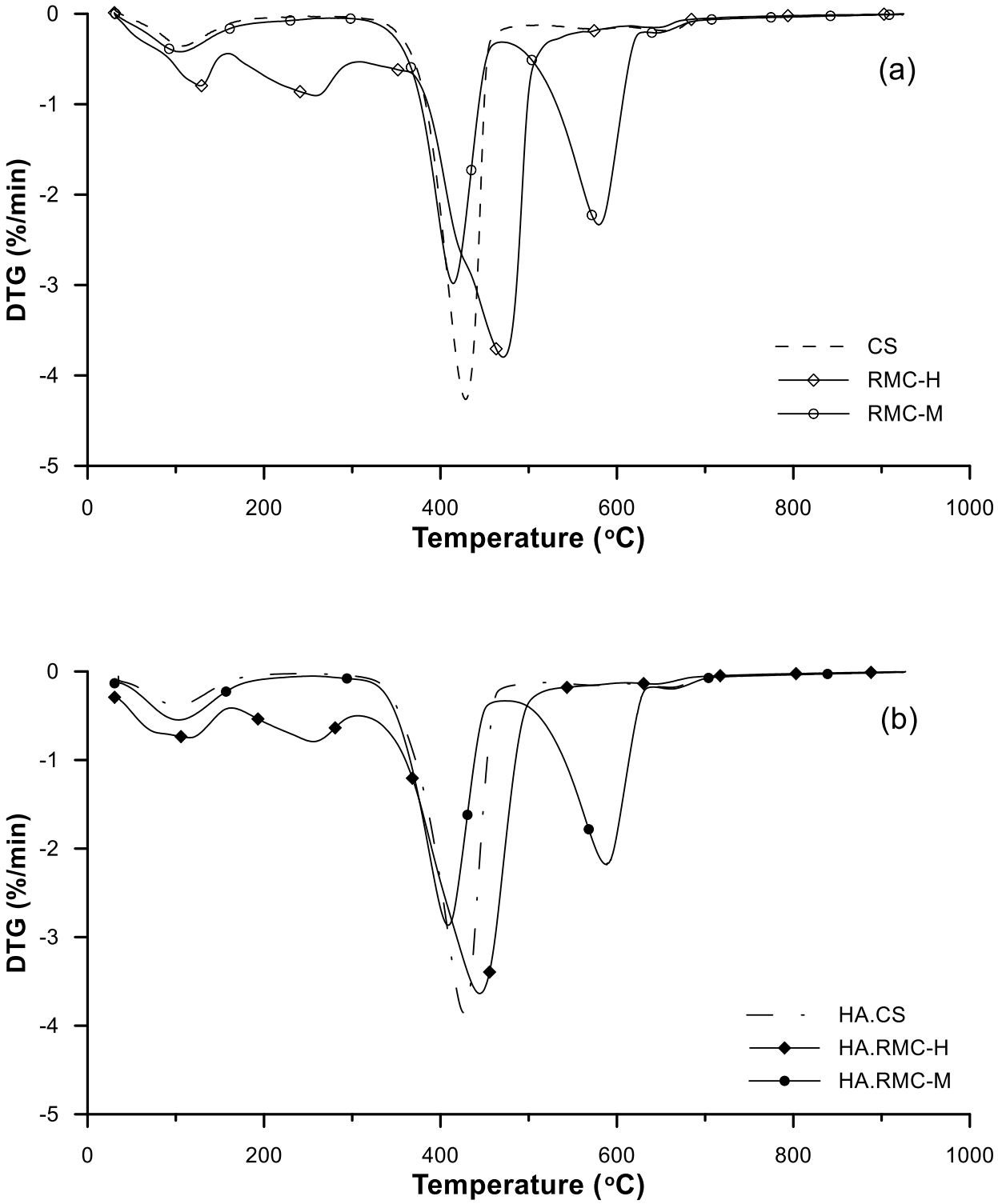

Fig. 20. DTG curves of samples cured under ambient conditions for 2 days, followed by accelerated carbonation conditions for 26 days: (a) without HA and (b) with HA